Magnetized spherically symmetric accretion flows

Roman Shcherbakov

Harvard University, Astronomy Department, 60 Garden Street, Cambridge, MA 02138

rshcherbakov@cfa.harvard.edu

30th August 2007

Abstract

Accretion onto compact objects is a challenging problem. The first averaged model was developed 55 years ago, but the theory is yet far from being complete. The real accretion was found to be time-dependent and turbulent. This paper presents the first averaged MHD spherical accretion model that separately deals with turbulence.

Turbulence treatment is based on simulations of several regimes of collisional MHD. The effects of freezing-in amplification, dissipation, dynamo action, isotropization and constant magnetic helicity are self-consistently included. The assumptions of thermal equipartition and magnetic field isotropy are released. Correct dynamics of magnetized flow is calculated. Energy transfer in a form of diffusion, convection or radiation is not accounted for.

Two different types of accretion flows are found. The first type is a transonic non-rotating flow. The second type is a flow with effective transport of angular momentum outward. Non-rotating flow has an accretion rate several times smaller than Bondi rate, because turbulence inhibits accretion. Flow with angular momentum transport has accretion rate about 10-100 times smaller Bondi rate. The effects of highly helical turbulence, states of outer magnetization and different equations of state are discussed. The flows were found to be convectively stable on average, despite gas entropy increases inwards.

These solutions can be effectively applied to Radiatively Inefficient Accretion Flows. The proposed model has a small number of free parameters, but has attractive properties. Density in the non-rotating magnetized flow was found to be several times lower than density in non-magnetized accretion. This helps to naturally explain the observed low IR luminosity and low Faraday rotation measure of accretion onto Sgr A*.

Subject headings: accretion, MHD, turbulence – Galaxy: center

1. Introduction

Dynamics of magnetized accretion flows is the major topic of astrophysical research. The problem can be solved with two different approaches: numerical and analytical. Each of them has specific difficulties, so that methods can be applied complementary.

Realistic numerical simulations require a lot of computational time to model even the isotropic case (Lazarian 2006). Convergence of properties of the isotropic turbulence is reached only when computational domain has more than 1024^3 cells (Ladeinde & Gaitonde 2004), (Biskamp 2003). Non-isotropic simulations of this scale were not performed. It is also very difficult to model the system with large range of scales. The system then possesses vastly different timescales. Existing simulations of accretion flows are either axisymmetric (McKinney 2006) or consider very small domain (Igumenshchev 2006). In addition, simulations should be run for sufficiently long time or several runs should be made to obtain average quantities, e.g. accretion rate, power of emitted radiation.

Analytical models do not suffer from a need to average, if they are based on averaged quantities. Most of them are. However, to build a reasonable model is itself difficult. No unified method exists to combine insights in physics and mathematics into a perfect analytical model. That is why the zoo of models of astrophysical flows is so huge.

In particular, many analytical treatments were devised for accretion: spherically symmetric treatment (Bondi 1952), (Coker & Melia 2000), (Beskin & Karpov 2005), standard disk (Shakura & Sunyaev 1973), Advection-Dominated Accretion Flow (Narayan & Yi 1995) with its variation Hot Luminous Accretion Flow (Yuan 2001), Adiabatic Inflow-Outflow Solutions (Blandford & Begelman 1999), Convection Dominated Accretion Flow (Narayan, Igumenshchev, & Abramowicz 2000), (Quataert & Gruzinov 2000), Jet-ADAF (Yuan, Quataert, & Narayan 2003). They are aimed to describe essentially the same process: axisymmetric plasma inflow onto a compact source. Some models include the effects the others miss. Energy transport in CDAF, outflows in ADIOS are the examples. Some effects are not treated properly in any model.

Magnetic field is a main source of uncertainty and mistakes in models of accretion flows. Two assumptions are usually posed to incorporate it into the model. Firstly, magnetic field is considered to be isotropic (Coker & Melia 2000), (Narayan & Yi 1995) or have some predominant direction (Scharlemann 1983). Then magnetic pressure and magnetic energy density may be put (Narayan & Yi 1995) into the dynamical equations. Secondly, the ratio of magnetic field energy density to gas thermal energy density is set to constant. This is called thermal equipartition assumption. These two ideas are at least unproven or may even not work. Magnetic field is predominantly radial in spherical inflow (Schwartzman 1971) because of freezing-in condition and predominantly toroidal in disk (Hawley & Balbus 2002) because of Magneto-Rotational Instability.

In a good model direction and strength of magnetic field should be determined self-consistently. Non-isotropy of magnetic field requires special dynamics. Dynamical equations were partially derived more than 20 years ago (Scharlemann 1983), but did not receive much attention or were even considered erroneous (Beskin & Karpov 2005).

Such a model may offer a natural explanation of certain accretion patterns. Accretion onto Sgr A* gives an excellent opportunity for testing. Our Galaxy is proven to host a Supermassive Black Hole (SMBH) named Sgr A* in its center (Ghez et al. (2003), Zhi-Qiang Shen (2006)).

This black hole accretes matter and emits radiation with characteristic low-luminosity spectrum (Narayan et al. 1998). This spectrum was satisfactory explained with the combination of two models: jet or non-thermal (Yuan, Quataert, & Narayan 2003) radio-emission and X-Rays with IR radiation coming from conventional ADAF flow. However, the large number of free parameters allows one to fit any spectrum satisfactory well. Model with no free parameters left is an ultimate goal of the ongoing study.

Partial progress in building a self-consistent accretion model is made in this paper, which is organized as follows. Basic spherical model is described in Section 2. Necessary boundary conditions are discussed in Section 3 for general flow and for Sgr A*. Results in Section 4 are followed by the discussion of the model in Section 5. Observational implications in Section 6 are supplemented with prospects for future work and Conclusion in Section 7. Paper has several appendices.

2. Spherical Model

Spherical accretion is the simplest pattern from all symmetric setups. We need to solve the basic model first to move then to a more realistic pattern. Construction of this maximally symmetric model is the topic of the following study.

Spherical coordinates (r, θ, ϕ) are used as a natural coordinate system for the spherical problem. Only averages of quantities are of interest. I average all the quantities over angular variables (θ, ϕ). The results depend only on the radial variable r in the assumption that angular averaging is the same as time averaging. I need now to determine the essential quantities and derive the closed system of equations for them.

Essential quantities of non-magnetized solution (Bondi 1952) are the inflow speed $v(r)$, density $\rho(r)$ and temperature $T(r)$. Magnetized case requires several more. As I release the assumption of isotropy, there are two special directions: along the radial vector $\vec{e_r}$ and perpendicular to the radial vector. To describe realistic Magneto Hydrodynamic turbulence, I need at least 6 quantities: squares of radial and perpendicular magnetic fields B_r^2 and $B_\perp^2$, squares of radial and perpendicular fluid motions u^2 and $u_\perp^2$, characteristic length scale L and dimensionless magnetic helicity δ. The last quantity will be described in detail in the corresponding subsection 2.4. For simplicity I consider random velocity to be isotropic and denote it as $u(r)$. I will later justify this isotropy assumption.

I base all calculations on Ideal Magneto Hydrodynamic system of equations (Landau, Lifshitz & Pitaevskii 1984). However, viscous terms are retained where they do not vanish in the limit of vanishing viscosity. The quantities in the following equations are fully dependent on time and coordinates. General mass flux equation reads

$$\frac{\partial \rho}{\partial t} + \vec{\nabla} \cdot (\rho \vec{V}) = 0, \tag{1}$$

where $\vec{V}$ is fluid velocity. Force balance is described by Navier-Stokes equation

$$\frac{\partial \vec{V}}{\partial t} + (\vec{V}\cdot\vec{\nabla})\vec{V} = -\frac{\vec{\nabla}p}{\rho} - \vec{\nabla}\phi_{\rm g} - \frac{[\vec{B}\times[\vec{\nabla}\times\vec{B}]]}{4\pi\rho} + \nu\triangle\vec{V}, \tag{2}$$

where $\phi_{\rm g}$ is gravitational potential, ν is kinematic viscosity. The magnetic term is Lorentz force density $F = [\vec{j}\times\vec{B}]/(c\rho)$ with current density $\vec{j} = c[\vec{\nabla}\times\vec{B}]/(4\pi)$. The last term is responsible for finite energy dissipation through Kolmogorov cascade (Landau & Lifshitz 1987). Momentum equation is a combination of (1) and (2)

$$\frac{\partial(\rho V_i)}{\partial t} = -\frac{\partial}{\partial x_k}\left(p\delta_{ik} + \rho V_i V_k + \frac{1}{4\pi}\left(\frac{1}{2}B^2\delta_{ik} - B_i B_k\right)\right) - \frac{\partial\phi_{\rm g}}{\partial x_i} + \nu(\triangle\vec{V})_i. \tag{3}$$

Energy equation includes information about the equation of state and cannot be derived directly from the above equations

$$\frac{\partial}{\partial t}\left(\frac{\rho V^2}{2} + \rho\varepsilon + \frac{B^2}{8\pi}\right) = -\vec{\nabla}\cdot\left(\rho\vec{V}\left(\frac{V^2}{2} + \phi_{\rm g} + w\right) + \frac{1}{4\pi}[\vec{B}\times[\vec{V}\times\vec{B}]] + \text{viscous}\right), \tag{4}$$

where ε is gas internal energy density, $w = \varepsilon + \int dp/\rho$ is gas specific enthalpy. Viscous terms have contributions proportional to kinematic viscosity ν, thermal diffusivity ξ and magnetic viscosity ν_M. They are responsible for diffusion. Magnetic field evolution is described by induction equation

$$\frac{\partial\vec{B}}{\partial t} = \vec{\nabla}\times[\vec{V}\times\vec{B}] + \nu_M\triangle\vec{B}. \tag{5}$$

Magnetic field does not have sources and is solenoidal

$$\vec{\nabla}\cdot\vec{B} = 0. \tag{6}$$

Random velocity field is also solenoidal for incompressible turbulence

$$\vec{\nabla}\cdot\vec{u} = 0. \tag{7}$$

2.1. Dynamics

Let me start deriving the system of equations on averages from general equations. Total velocity of a fluid parcel

$$\vec{V}(r,\theta,\phi,t) = v(r)\vec{e}_r + \vec{u}(r,\theta,\phi,t) \tag{8}$$

is a sum of averaged inflow speed $v(r)$ and instantaneous random velocity $u(r,\theta,\phi,t)$, where by definition angular average of turbulent velocity vanishes

$$\int \vec{u}(r,\theta,\phi,t)d\Omega = 0. \tag{9}$$

General continuity equation (1) can be averaged with the aid of (7) and (9) to

$$\rho(r)v(r)r^2 = \dot{M}, \tag{10}$$

where $\dot{M}$ is the mass accretion rate.

Averaged force equation is more convenient to derive from general momentum equation (3). Tensor $\rho V_i V_k$ averages out into the diagonal form $\rho v^2 \delta_{rr} + \rho u^2 \delta_{ik}/3$. Because there are no sources of magnetic field (6) and spherical geometry is assumed, no regular magnetic field exist. Following (Scharlemann 1983), I add $B_r \nabla \cdot \vec{B}/(4\pi\rho)$ to the radial magnetic force $F_r = [\vec{B} \times [\vec{\nabla} \times \vec{B}]]_r/(4\pi\rho)$, average over the solid angle and then set $B_\phi = B_\perp$ and $B_\theta = B_\perp$. Cross-terms with $B_\theta \cdot B_r$, $B_\phi \cdot B_r$ and $B_\phi \cdot B_\theta$ cancel on average over the solid angle. Finally, I obtain

$$F_r = \frac{(r^4 B_r^2)'_r}{8\pi\rho r^4} - \frac{(r^2 B_\perp^2)'_r}{4\pi\rho r^2} \tag{11}$$

for the magnetic force. I denote by $()'_r$ radial derivatives. I omit bulk viscosity term that results from $\nu\triangle\vec{V}$. Paczynski-Wiita gravitational potential (Paczhynski & Wiita 1980)

$$\phi_{\rm g} = -\frac{r_{\rm g} c^2}{2(r - r_{\rm g})} \tag{12}$$

is used to imitate the effects of General Relativity, where

$$r_{\rm g} = \frac{2GM}{c^2} \tag{13}$$

is a Schwarzschild radius of an object with mass M. I take gas pressure to be that of an ideal gas $p = \rho RT/\mu$, where μ is a mean molecular weight. Combining all the terms and using (10), I come to the averaged equation for forces

$$v v'_r + \frac{r_{\rm g} c^2}{2(r - r_{\rm g})^2} + \frac{R}{\mu}\frac{(\rho T)'_r}{\rho} + \frac{(\rho u^2)'_r}{3\rho} + \frac{(r^2 B_\perp^2)'_r}{4\pi\rho r^2} - \frac{(r^4 B_r^2)'_r}{8\pi\rho r^4} = 0. \tag{14}$$

Averaged energy advection equation can be derived directly from general energy equation (4). Enthalpy term should include contribution from random fluid motions as well as from gas. Isotropic random motions of fluid exert isotropic pressure $p_{\rm rand} = \rho u^2/3$ and have the internal energy density $\varepsilon_{\rm rand} = u^2/2$. Total enthalpy w is

$$w = w_{\rm gas} + w_{\rm rand}, \quad \text{where} \quad w_{\rm gas} = \frac{RT(f_e \cdot a_e(T) + f_i \cdot a_i(T) + 1)}{\mu} \quad \text{and} \quad w_{\rm rand} = \frac{5}{6}u^2. \tag{15}$$

Fractions of electrons $f_e \approx 0.54$ and ions $f_i \approx 0.46$ are calculated for a gas with twice solar abundance of elements. Such high concentration of helium and metals was assumed by (Baganoff et al. 2003) for spectrum fitting. Correspondent mean molecular weight is $\mu \approx 0.7 {\rm g} \cdot {\rm cm}^{-3}$. Integral heat capacity per particle $a_e(T)$ and $a_i(T)$ are different for electrons and ions. Ions are non-relativistic down to $r_{\rm g}$ (Narayan & Yi 1995). Therefore $a_i(T) = 3/2$. General expression (Chandrasekhar 1939) should be used for thermal relativistic electrons $a_e(T) = \Theta^{-1}(3K_3(\Theta^{-1}) + K_1(\Theta^{-1})/(4K_2(\Theta^{-1})) - 1)$. Here $\Theta = kT/m_e c^2$ is dimensionless temperature, $K_x(Y)$ are modified Bessel functions of the second kind. Expression for non-relativistic enthalpy is

$$w_{NR} = \frac{5RT}{2\mu} + \frac{5}{6}u^2. \tag{16}$$

It is valid in the limit $\Theta \ll 1$. Stationary energy equation is obtained from (4) by setting all time derivatives to zero. It takes a form $\vec{\nabla}\vec{q} = 0$, where $\vec{q}$ is energy flux. Part of flux proportional to random velocity $\vec{u}$ averages out, because turbulence is incompressible and u is zero on average (9). Applying continuity (10) relation, I finally obtain

$$vv'_r + \frac{r_g c^2}{2(r-r_g)^2} + w'_r + \frac{1}{2\pi}\left(\frac{B_\perp^2}{\rho}\right)'_r = 0, \tag{17}$$

where again $B_\theta^2 = B_\phi^2 = B_\perp^2$. I assumed the term $\int [\vec{B} \times [\vec{u} \times \vec{B}]] d\Omega$ to also be zero along with all viscous energy transfer terms. I limit this study to Advection Dominated flows by deliberately cutting off diffusion and convection (see Appendix D).

Subtracting force equation (14) from energy advection equation (17) I get the heat balance equation that reads in non-relativistic limit

$$\frac{R}{\mu}\left(\frac{3}{2}T'_r - \frac{\rho'_r}{\rho}T\right) + \left(\left(\frac{u^2}{2}\right)'_r - \frac{\rho'_r}{\rho}\frac{u^2}{3}\right) + \frac{\rho r^2}{4\pi}\left(\frac{B_\perp^2}{\rho^2 r^2}\right)'_r + \frac{1}{8\pi\rho r^4}(r^4 B_r^2)'_r = 0, \tag{18}$$

similar to entropy conservation in hydrodynamics. Work done by gas is represented by $-\rho'_r/\rho T$. The first term has exactly the form of the second, if I make the substitution of the mean square particles velocity

$$v_p^2 = \frac{3RT}{\mu}. \tag{19}$$

Work done by the magnetic field enters the expression as the derivatives of ρ and r in the magnetic part.

2.2. Evolution of turbulence

Dynamics is the only part of ideal Bondi problem (Bondi 1952). In reality, flow always has some turbulence that exerts back-reaction on the flow. The magnitude of back-reaction terms should be determined from additional equations that describe the evolution of turbulence. Since no complete theory of turbulence exists, I make a lot of approximations. The model is adjusted to agree with the results of certain numerical simulations. I also apply analytical tests to assure the model reproduces the basic properties of observed turbulence.

I need non-ideal induction equation (5) and Navier-Stokes equation (2) to derive how turbulence evolves. My goal is to compound reasonable equations on average squares of radial magnetic field B_r^2, perpendicular magnetic field $B_\perp^2$, isotropic velocity u^2. I also need equations on characteristic length scale of turbulence L and dimensionless magnetic helicity δ.

Radial part of induction equation (5) easily gives the equation on B_r^2, when the former is multiplied by $2B_r$ and averaged over the solid angle.

$$2B_r\frac{\partial B_r}{\partial t} = 2B_r[\vec{\nabla} \times [v\vec{e}_r \times \vec{B}]]_r + 2B_r[\vec{\nabla} \times [\vec{u} \times \vec{B}]]_r + 2\nu_M B_r(\triangle\vec{B})_r \tag{20}$$

where indices $()_r$ without prime denote just the radial part. The left-hand side vanishes, because the square average does not depend on time. The first term on the right-hand side represents the

uniform increase of magnetic field due to flux freezing. I combine it with the continuity equation (10) to eliminate v derivatives. The second terms is the dynamo action. It cannot be easily averaged. Characteristic turbulence length scale L may be used to approximate derivatives

$$\frac{\partial B_i}{\partial x_k} \sim \frac{B_i}{L}\vec{e}_k \quad and \quad \frac{\partial u_i}{\partial x_k} \sim \frac{u_i}{L}\vec{e}_k. \tag{21}$$

Then we arrive at dynamo action with characteristic timescale $\tau_{\rm dyn}$ about eddy turn-over time $\tau_{\rm edd} = u/L$. Averaging of the second term gives quadratic in magnetic field expression. I set timescale coefficient c_{Bu1} for same-direction correlation B_iB_i and c_{Bu2} for any B_iB_k, with $i \neq k$. I expect equal contributions from $B_r \cdot B_\theta$ and $B_r \cdot B_\phi$. The final expression reads $2B_r[\vec{\nabla} \times [\vec{u} \times \vec{B}]]_r \sim (c_{Bu1}B_r^2 + c_{Bu2}B_r(B_\theta + B_\phi))u/L$. Characteristic

$$B_r = \sqrt{B_r^2} \quad \text{and} \quad B_\theta = B_\phi = B_\perp = \sqrt{B_\perp^2} \tag{22}$$

are taken. The last term on the right-hand side of (20) represents magnetic field dissipation. Dissipation term $\nu_M \triangle \vec{B}$ of induction equation (5) is macroscopic in turbulence even for vanishing magnetic diffusivity ν_M (Biskamp 2003). Dissipation has a timescale $\tau_{\rm dyss}$ about Alfven timescale $\tau_A = v_A/L$. Averaging of the last term also gives quadratic form in magnetic field. I set timescale coefficient c_{BB1} for same-direction correlation B_iB_i and c_{BB2} for any B_iB_k, $i \neq k$. Finally, $\nu_M B_r(\triangle \vec{B})_r \sim v_A(c_{BB1}B_r^2 + c_{BB2}(B_\theta + B_\phi)B_r)/L$. I take v_A to be that in the direction of interest, eliminating some freedom of form of the dissipation term. Collecting all the terms, I obtain

$$\frac{v}{r^4}\frac{\partial(B_r^2 r^4)}{\partial r} = \frac{-(c_{Bu1}B_r^2 + 2c_{Bu2}B_rB_\perp)u + (c_{BB1}B_r^2 + 2c_{BB2}B_rB_\perp)v_{Ar}}{L} \tag{23}$$

for the radial magnetic field in the absence of external energy sources. Radial v_{Ar} and perpendicular $v_{A\perp}$ Alfven speeds and random velocity u are

$$v_{Ar} = \frac{\sqrt{B_r^2}}{\sqrt{4\pi\rho}}, \qquad v_{A\perp} = \frac{\sqrt{B_\perp^2}}{\sqrt{4\pi\rho}}, \qquad u = \sqrt{u^2}. \tag{24}$$

Coefficients $c_{Bu1}, c_{Bu2}, c_{BB1}, c_{BB2}$ are yet to be determined.

Perpendicular part of induction equation (5), for example θ part, gives the equation on B_θ^2 when (5) is multiplied by B_θ and averaged over the solid angle. The flux freezing condition for perpendicular field is different from that for radial field: $B_\theta vr = $ const represents perpendicular flux freezing. I repeat the calculations made for radial field B_r to find dynamo and dissipation terms. Dynamo term takes form $(c_{Bu1}B_\theta^2 + c_{Bu2}B_\theta(B_\phi + B_r))u/L$. Dissipation is $v_{A\theta}(c_{BB1}B_\theta^2 + c_{BB2}(B_\phi + B_r)B_\theta)/L$. Here I take $B_\perp^2 = B_\theta^2 = B_\theta B_\phi = B_\phi^2$. Finally, I obtain

$$v\rho^2 r^2 \frac{\partial}{\partial r}\left(\frac{B_\perp^2}{\rho^2 r^2}\right) = \frac{-((c_{Bu1} + c_{Bu2})B_\perp^2 + c_{Bu2}B_\perp B_r)u + ((c_{BB1} + c_{BB2})B_\perp^2 + c_{BB2}B_\perp B_r)v_{A\perp}}{L}, \tag{25}$$

where continuity equation (10) is used.

Evolution equation for squared random fluid velocity u^2 can be derived from momentum equation (3), when it is multiplied by $2\vec{u}$ and averaged over the solid angle. Potential energy

and pressure terms average out and only three terms are left

$$2\vec{u}\left((\vec{V}\vec{\nabla})\vec{V}+\frac{\vec{\nabla}(\rho V)}{\rho}\right)=2\frac{\vec{u}[\vec{B}\times[\vec{\nabla}\times\vec{B}]]}{4\pi\rho}+2\vec{u}\nu\triangle\vec{u}. \tag{26}$$

I apply the same averaging procedure as during the derivation of magnetic field evolution equations (23) and (25). The last term is finite in turbulence even for vanishing viscosity ν (Landau & Lifshitz 1987). I expect the first term on the right-hand side of (26) to give equal contribution with coefficient c_{uB1} from every B_i^2 and equal contribution with c_{uB2} from every correlation B_iB_k for $i\neq k$, such that the whole term equals $(c_{uB1}(v_A^2+2v_{A\perp}^2)+c_{uB2}(2v_Av_{A\perp}+v_{A\perp}^2))u/L$. The final result is

$$v\rho^{2/3}\frac{\partial}{\partial r}\left(\frac{u^2}{\rho^{2/3}}\right)=\frac{c_{uu}u^3-(c_{uB1}v_A^2+(2c_{uB1}+c_{uB2})v_{A\perp}^2+2c_{uB2}(v_Av_{A\perp}))u}{L}, \tag{27}$$

with other three coefficients c_{uu}, c_{uB1} and c_{uB2}. Some of these and other c_{xx}-like coefficients can be taken from numerical simulations of isotropic turbulence, some of them can be inferred from analytical tests.

2.3. Correspondence to numerical simulations

Isotropic turbulence is studied quite thoroughly in numerical simulations. Some results are reproduced by a number of researchers (see (Biskamp 2003) for the review). That is why we may believe in these results and base a model on them. Three simulations of different turbulence regimes turbulence can provide four conditions that let us uniquely determine four combinations of coefficients c_{xx}. These regimes are decaying HD turbulence, decaying MHD turbulence and dynamo growth of small seed magnetic field. I assume then that c_{xx} are constants independent on regime and extend the derived model to any anisotropic case.

Let me consider my model in isotropic incompressible case of box turbulence. In this settings $B_r^2=B_\theta^2=B_\phi^2$. Squared magnetic field B^2 equals $B^2=3B_r^2$. Transition to the co-moving frame of averaged inflow in turbulence evolution equations (23), (25), (27) is done by stating $d/dt=-v\partial/\partial r$. Now I should write time derivative instead of radius derivative and set $r=\text{const}$, since matter is not moving anywhere from the box. I obtain equations of evolution of the isotropic turbulent Alfven speed v_A and isotropic turbulent velocity u:

$$\left(u^2\right)_t'=\frac{\hat{c}_{uB}v_A^2u-\hat{c}_{uu}u^3}{L},\qquad \left(v_A^2\right)_t'=\frac{\hat{c}_{Bu}v_A^2u-\hat{c}_{BB}v_A^3}{L}. \tag{28}$$

Here $v_A=\sqrt{B^2}/\sqrt{4\pi\rho}$ and $\rho=\text{const}$. Coefficients with hats are

$$\begin{aligned}\hat{c}_{Bu}&=c_{Bu1}+2c_{Bu2}, & \hat{c}_{BB}&=\frac{c_{BB1}+2c_{BB2}}{\sqrt{3}},\\ \hat{c}_{uu}&=c_{uu1}, & \hat{c}_{uB}&=c_{uB1}+c_{uB2}\end{aligned} \tag{29}$$

in terms of previously defined c_{xx}.

I have a freedom to set L, because it enters the equations only in combinations c_{xx}/L, but c_{xx} are not yet determined. For simplicity of further derivation I take $L(r)$ to be the size of energy containing eddies for isotropic incompressible turbulence:

$$u^2 = \int^{\frac{2\pi}{L}} (u^2)_k dk \quad \text{and} \quad v_A^2 = \int^{\frac{2\pi}{L}} (v_A^2)_k dk. \tag{30}$$

Isotropic decay of hydrodynamic turbulence is the simplest simulation. The convenient constant of decay is Kolmogorov constant C_{HD}. It is defined as

$$C_{HD} = E_k k^{5/3} \epsilon^{-2/3} \quad \text{with} \quad \epsilon = -\frac{d}{dt}\left(\frac{u^2}{2}\right) \quad \text{and} \quad E_k = \frac{(u^2)_k}{2}, \tag{31}$$

where E_k is energy spectrum, ϵ is a decay rate. Kolmogorov constant was found to be $C_{HD} \approx 1.65$ in the large set of simulations (Sreenivasan 1995). I substitute this number into (31) and evaluate the first integral in (30) to find

$$\hat{c}_{uu} = \frac{4\pi}{(3C_{HD})^{3/2}} \approx 1.14 \tag{32}$$

for isotropic equations (28).

Isotropic decay of magneto hydrodynamic turbulence gives two conditions. MHD Kolmogorov constant has similar to (31) definition

$$C_{MHD} = E_k k^{5/3} \epsilon^{-2/3} \quad \text{with} \quad \epsilon = -\frac{d}{dt}\left(\frac{u^2 + v_A^2}{2}\right) \quad \text{and} \quad E_k = \frac{(u^2)_k + (v_A^2)_k}{2}. \tag{33}$$

MHD turbulence is more difficult to model numerically, but the value of $C_{MHD} \approx 2.2$ is rather rigorous (Biskamp 2003). In addition, kinetic energy was found to decay in exactly the same rate as magnetic energy. Evaluation of the sum of two integrals (30) with definitions (33) and known C_{MHD} yields

$$\hat{c}_{BB} - \hat{c}_{Bu} = \hat{c}_{uu} - \hat{c}_{uB} \approx 2\pi \left(\frac{2}{3C_{MHD}}\right)^{3/2} \approx 1.05. \tag{34}$$

Dynamo simulations explore the regime $v_A^2 \ll u^2$. Exponential growth of small magnetic field corresponds to some value of coefficient $\hat{c}_{Bu}$ in (28):

$$B^2 \propto \exp\left(\hat{c}_{Bu}\frac{ut}{L}\right) \tag{35}$$

External driving is purely mechanical for $v_A^2 \ll u^2$, so external source of magnetic field does not alter the picture of field amplification by dynamo. Characteristic length scale in dynamo simulations is usually the size of energy containing eddies L consistent with (30), so renormalization of length scale is not required. Older simulations (Kida, Yanase, & Mizushima 1991) have found $b = 0.39$ for simulations with highest resolution that corresponds to $\hat{c}_{Bu} \approx 0.61$.

Later results (Schekochihin et al. 2004) indicate a bit higher value $\hat{c}_{Bu} \approx 0.7$ that I will use for my model. Finally,

$$\begin{aligned} \hat{c}_{Bu} &= 0.70, \qquad \hat{c}_{BB} = 1.75, \\ \hat{c}_{uu} &= 1.14, \qquad \hat{c}_{uB} = 0.09. \end{aligned} \tag{36}$$

The values of four $\hat{c}_{xx}$ (36) are not enough to obtain all seven coefficients c_{xx} in (23), (25), (27) with definitions (29). However, the application of common sense analytical conditions to non-isotropic system of equations puts some additional constrains on c_{xx} that allows me to complete the model with as little guessing as possible.

Analytic tests are described in Appendix A. This completes the derivation and verification of turbulence evolution equations (23), (25), (27) with coefficients

$$\begin{aligned} c_{BB1} &= 3.03, \qquad c_{BB2} = 0.00, \qquad c_{Bu1} = 0.41, \qquad c_{Bu2} = 0.29 \\ c_{uu} &= 1.14, \qquad c_{uB1} = 0.09, \qquad c_{uB2} = 0.00 \end{aligned} \tag{37}$$

that I obtain summarizing (29), (36), (A11) and (A12). However, not all major effect have been included so far.

2.4. Magnetic helicity

Certain correlation called "magnetic helicity" may strongly influence magnetic field dissipation. This quantity is defined as

$$H = \int_V (\vec{A} \cdot \vec{B}) dV, \tag{38}$$

where $\vec{A}$ is a vector potential with a defined gauge condition (Biskamp 2000). Time derivative of magnetic helicity is very small compared to the time derivative of magnetic energy in high Re astrophysical plasma (Biskamp 2003)

$$\frac{dH}{dE_M} \frac{E_M}{H} \lll 1. \tag{39}$$

Constancy of magnetic helicity defines the rules of selective decay. Magnetic energy E_M decays in free turbulence down to non-zero value, allowed by constant magnetic helicity $H =$ const. The final force-free configuration has zero random kinetic energy E_K and has aligned current density and magnetic field $\vec{j} \uparrow\uparrow \vec{B}$ (Biskamp 2003). Magnetic field does not exert any force on matter because of this alignment.

However, the derived system of turbulence evolution equations (A1) and, therefore, (23), (25), (27) cannot handle selective decay. Decay of magnetic energy must be modified. I need to have the transition to zero dissipation rate at certain v_{Ar} and $v_{A\perp}$ as a function of magnetic helicity H. First, I should employ the proper magnetic helicity constancy. Then I should quantify the relation between critical v_{Ar}, $v_{A\perp}$ and H.

Let me consider the region S that evolves together with the mean flow of fluid. This region has the constant angle boundaries $\theta = \text{const}$ and $\phi = \text{const}$. Its radial elongation L_r scales as inflow velocity: $L_r \propto v$. The region S contains constant mass $m = \text{const}$ of matter, because matter flux through its boundaries is zero by definition. If I neglect diffusion by random velocity, frozen magnetic field lines do not move through the boundaries of the region. Because of this (Biskamp 2003), magnetic helicity in S is constant $H = \text{const}$.

The simplest order of magnitude relation between magnetic energy E_M and H is

$$E_M \cdot L_H = H = \text{const} \tag{40}$$

in the region S, where L_H is magnetic helicity characteristic length scale (Biskamp 2003). As magnetic field decays in turbulence, L_H grows according to (40).

I can parametrize L_H to be a fraction of L :

$$L_H = \xi L. \tag{41}$$

Volume of the region of interest S is

$$V = \frac{m}{\rho} \tag{42}$$

with $m = \text{const}$. Total magnetic energy E_M is

$$E_M = \frac{1}{8\pi}(B_r^2 + 2B_\perp^2). \tag{43}$$

I substitute (41), (42) and (43) into (40) and use the definition (24) of Alvfen velocities to come to

$$L(v_{Ar}^2 + 2v_{A\perp}^2)\xi = \text{const}. \tag{44}$$

Now I need to include ξ into the turbulence evolution equations (23), (25), (27) so that they can handle selective decay. The natural limit of L_H growth is the characteristic size of energy containing large eddies L. So regime $\xi \ll 1$ corresponds to non-helical turbulence and regime $\xi \sim 1$ to turbulence, where magnetic helicity significantly inhibits dissipation. Regime $\xi > 1$ does not occur. The basic way to modify the equations is to decrease by a smooth multiplier $f(\xi) < 1$ magnetic field decay rate. For qualitative agreement with experiment (Biskamp 2003) I can employ

$$f(\xi) = \exp(-\xi), \tag{45}$$

what means that magnetic energy dissipation timescale becomes $\exp(\xi)$ times larger. Terms with both u and v_{Ar} or $v_{A\perp}$ in magnetic field evolution do not need to be modified, since random velocity energy decays to zero and these terms do not matter. However, I multiply the term with both random velocity and Alfven speed by $\exp(-\xi)$ to make random velocity u decay to zero.

I come to exactly the same expression (44) in a more rigorous approach, when I consider flux tubes (see Appendix B).

2.5. System of equations with source terms

With only minor corrections, the final system of equations can be written down. In general, turbulence has external sources of energy that sustain finite magnetic and kinetic energies even in case of box turbulence. I can add source terms to incompressible system (A1) and consequently to the system of compressible equations (23), (25), (27).

System (A1) with coefficients (36) and (37), modifier (45) and source terms reads

$$\frac{d(v_{Ar}^2)}{dt} = \frac{(0.70v_{Ar}^2 + 0.58(v_{A\perp} - v_{Ar})v_{Ar})u - 3.03v_{Ar}^3\exp(-\xi)}{L} + c_0\frac{v_p^3}{L}, \tag{46a}$$

$$\frac{d(v_{A\perp}^2)}{dt} = \frac{(0.70v_{A\perp}^2 + 0.29(v_{Ar} - v_{A\perp})v_{A\perp})u - 3.03v_{A\perp}^3\exp(-\xi)}{L} + c_1\frac{v_p^3}{L}, \tag{46b}$$

$$\frac{d(u^2)}{dt} = \frac{0.09(v_{Ar}^2 + 2v_{A\perp}^2)u\exp(-\xi) - 1.14u^3}{L} + c_2\frac{v_p^3}{L}, \tag{46c}$$

where v_p is the mean square particles speed (19) and c_0, c_1 and c_2 are dimensionless coefficients. These coefficients determine the rates of energy transfer into different turbulent fields.

I can parameterize the total turbulent energy with σ_∞. I take it to be the ratio of total turbulent energy to thermal energy

$$\sigma = \frac{E_K + E_M}{E_{\rm th}}, \quad \text{so that} \quad \sigma_\infty\frac{3RT}{2\mu} = \sigma\frac{v_p^2}{2} = \frac{u^2}{2} + \frac{v_{Ar}^2}{2} + v_{A\perp}^2. \tag{47}$$

Magnetization parameter σ with definition (47) is somewhat similar to conventional plasma magnetization parameter, but the conventional magnetization does not include energy of random fluid motions.

In the dynamic equilibrium of constant v_{Ar}, $v_{A\perp}$, u and known ξ system (46) gives three algebraic equations for ratios v_{Ar}/v_p, $v_{A\perp}/v_p$ and u/v_p as functions of c_0, c_1 and c_2. To estimate c_0, c_1 and c_2 I take stationary driven isotropic turbulence with kinetic energy E_K equal to magnetic energy E_M. Isotropic turbulence of interest has $v_{Ar} = v_{A\perp} = u/\sqrt{3}$. Such turbulence occurs far from the central object, where outer magnetization is constant $\sigma_i nfty$. Solving (46) I obtain using (47)

$$c_0 = c_1 \approx 0.124\sigma_\infty^{3/2}, \qquad c_2 = 3c_0 \approx 0.371\sigma_\infty^{3/2} \tag{48}$$

in case $\xi = 0$. I apply these values even to turbulence with $\xi > 0$.

Total energy input Q_+ into E_K and E_M is

$$Q_+ \approx 0.742\sigma_\infty^{3/2}\frac{v_p^3}{L}. \tag{49}$$

This energy adds up to thermal gas energy after being processed through turbulence. However, I do not adjust my dynamical equations (14) and (17) for Q_+. I self-consistently omit heating and radiative or diffusive cooling. This omission is physically justified sufficiently far from the central object, where cooling Q_- balances heating Q_+.

Only size L of energy containing eddies should be specified to complete the derivation of closed system of equations. In the case when energy input Q_+ does not matter, the problem has only one relevant scale that is the size of the system r. Therefore, I can set L to be the fraction of radius

$$L = \gamma r \tag{50}$$

with the proportionality constant γ about unity. However, energy input from external sources Q_+ is relatively large far from the central source. This causes medium with constant Q_+, constant v_p and constant σ_∞ to have constant size of largest eddies

$$L = L_\infty = \text{const} \tag{51}$$

because of (49). This equality holds for radii larger than some $r_0 \approx L_\infty/\gamma$. I introduce a function with a smooth transition from (50) for $r \ll r_0$ to (51) for $r \gg r_0$:

$$L(r) = L_\infty \left(1 - \exp\left(-\frac{\gamma r}{L_\infty}\right)\right) \tag{52}$$

This completes derivation and verification of 8 equations (10), (14), (17) (23),(25), (27), (44), (52)with all coefficients (36), (37) and (48) on 8 quantities $L(r)$, $\xi(r)$, $v(r)$, $u(r)$, $v_{Ar}(r)$, $v_{A\perp}(r)$, $T(r)$, $\rho(r)$ that are characteristic turbulent length scale, normalized magnetic helicity, matter inflow velocity, turbulent velocity, radial Alfven speed, 1-D perpendicular Alfven speed, temperature and density. I rewrite the equations once again in terms of named quantities:

$$\rho v r^2 = \dot{M}, \tag{53a}$$

$$v v_r' + \frac{r_\mathrm{g} c^2}{2(r - r_\mathrm{g})^2} + \frac{R}{\mu}\frac{(\rho T)_r'}{\rho} + \frac{(\rho u^2)_r'}{3\rho} + \frac{(r^2 \rho v_{A\perp}^2)_r'}{\rho r^2} - \frac{(r^4 \rho v_{Ar}^2)_r'}{2\rho r^4} = 0, \tag{53b}$$

$$v v_r' + \frac{r_\mathrm{g} c^2}{2(r - r_\mathrm{g})^2} + (w_g)_r' + \frac{5}{3} u u_r' + 2(v_{A\perp}^2)_r' = 0 \quad \text{with} \tag{53c}$$

$$w_{gR} = \frac{RT}{\mu}\left(0.54\frac{3K_3(\Theta^{-1}) + K_1(\Theta^{-1})}{\Theta(4K_2(\Theta^{-1}) - 1)} + 1.69\right) \quad \text{or} \quad w_{gNR} = \frac{5RT}{2\mu},$$

$$v\frac{(\rho v_{Ar}^2 r^4)_r'}{\rho r^4} = \frac{3.03 v_{Ar}^3 \exp(-\xi) - (0.70 v_{Ar}^2 + 0.58(v_{A\perp} - v_{Ar})v_{Ar})u}{L} - \frac{0.64}{L_\infty}\left(\frac{RT_\infty \sigma_\infty}{\mu}\right)^{3/2}, \tag{53d}$$

$$v\rho r^2 \left(\frac{v_{A\perp}^2}{\rho r^2}\right)_r' = \frac{3.03 v_{A\perp}^3 \exp(-\xi) - (0.70 v_{A\perp}^2 + 0.29(v_{Ar} - v_{A\perp})v_{A\perp})u}{L} - \frac{0.64}{L_\infty}\left(\frac{RT_\infty \sigma_\infty}{\mu}\right)^{3/2}, \tag{53e}$$

$$v\rho^{2/3}\left(\frac{u^2}{\rho^{2/3}}\right)_r' = \frac{1.14u^3 - 0.09(v_{Ar}^2 + 2v_{A\perp}^2)u\exp(-\xi)}{L} - \frac{1.93}{L_\infty}\left(\frac{RT_\infty \sigma_\infty}{\mu}\right)^{3/2}, \tag{53f}$$

$$L(v_{Ar}^2 + 2v_{A\perp}^2)\xi = 3L_\infty \xi_\infty \frac{RT_\infty \sigma_\infty}{\mu}, \tag{53g}$$

$$L = L_\infty \left(1 - \exp\left(-\frac{\gamma r}{L_\infty}\right)\right). \tag{53h}$$

Here $\Theta = kT/m_e c^2$. Since my prescription for external driving of turbulence is $Q_+ = \text{const}$, I take v_p and L to be constant in source term.

Two values of gas enthalpy w_g are taken: relativistic w_{gR} and non-relativistic w_{gNR}. Relativistic enthalpy describes the correct one-temperature equation of state (EOS), where electrons are treated as relativistic particles. Non-relativistic enthalpy describes the 1-T EOS with effectively non-relativistic electrons. The latter case is not self-consistent, but is widely used in the studies of accretion (Bondi 1952), (Shapiro & Teukolsky 1983), (Yuan et al. 2005). It corresponds to gas adiabatic index $\Gamma = 5/3$. In the next section I describe the values of boundary conditions and parameters for the equations I solve.

3. Boundary conditions and parameters

The system (53) consists of 5 differential and 3 algebraic equations and should be integrated inside from some outer boundary at r_x. This requires 8 boundary conditions. These are the values "at infinity" L_∞, T_∞, ρ_∞, ξ_∞, u_∞, $v_{Ar\infty}$, $v_{A\perp\infty}$ and $\dot{M}$. I assume isotropic turbulence at my outer boundary that contains equal amounts of kinetic E_K and magnetic E_M energies. Therefore

$$v_{Ar\infty} = v_{A\perp\infty} = \left(\frac{RT_\infty\sigma_\infty}{\mu}\right)^{1/2} \quad \text{and} \quad u_\infty = \left(\frac{3RT_\infty\sigma_\infty}{\mu}\right)^{1/2}, \tag{54}$$

and I have one parameter σ_∞ instead of 3 velocities $v_{Ar\infty}$, $v_{A\perp\infty}$, u_∞. Another adjustable parameter of the model is length scale parameter γ. Accretion rate $\dot{M}$ is usually determined by some extra condition and is not adjustable.

Parameter γ is not free, but its value cannot be determined within the proposed theory. Neither there exist anisotropic MHD simulations that could provide γ. All simulations to date show γ to be within $0.2 \div 2$ (Tennekes & Lumley 1972), (Landau & Lifshitz 1987), (Biskamp 2003) in both HD and MHD case. I assume the same range of γ in my calculations.

3.1. Outer medium transition

Bondi radius

$$r_B = r_\mathrm{g}\frac{c^2}{c_\infty^2} \quad \text{with} \quad c_\infty = \left(\frac{5RT_\infty}{3\mu}\right)^{1/2} \tag{55}$$

is the natural length scale of the spherical accretion flow (Bondi 1952). Density ρ and temperature T of plasma are constant for radii $r \gg r_B$, because gravitational energy and gas regular kinetic energy are negligible there compared to gas internal energy (Bondi 1952). Averaged magnetic field and averaged random velocity are also constant for $r \gg r_B$, because left-hand sides of equations (53d), (53e) and (53f) are much smaller than either of term on the right-hand

side. External energy input balances dissipation in this region. I can take $L = L_\infty$ and $\xi = \xi_\infty$ from (53g) at $r \gg r_B$.

I set the outer boundary at $r_x = 3r_B$, where matter is almost uniform. It is difficult to specify L_∞. It should be determined from known external energy input Q_+ and outer magnetization σ_∞. However, I assume for uniformity that behavior of L breaks at the same r_B as the behaviors of temperature and density, so that $r_0 = L_\infty/\gamma$ and finally

$$r_x = 3r_B, \qquad L_\infty = \gamma r_B. \tag{56}$$

Bondi radius is about $r_B \approx 3 \cdot 10^5 r_{\rm g}$ for our Galactic Center (Ghez et al. 2003). The properties of gas at $3r_B$ are somewhat constrained from observations. I take the values for uniformly emitting gas model with temperature $T_\infty \approx 1.5 \cdot 10^7$ K, electron and total number densities $n_{e\infty} = 26cm^{-3}$, $n_\infty = 48cm^{-3}$ (Baganoff et al. 2003) at $r_x = 3r_B$ that corresponds to $5''$ in the sky. The presence of dense cold component can make the average temperature much lower and the average density much higher (Cuadra et al. 2006), but I am leaving these uncertainties for future research.

Expanding and colliding hyperalfvenic stellar winds provide magnetic field into the region. Its strength near Bondi radius is not known. Only the very general estimate can be made. Matter magnetization is likely to be lower than the saturation value of $\sigma_\infty = 1$. I take the values in the range $\sigma_\infty = 0.001 \div 1$ to cover all reasonable magnetization states of matter at $3r_B$. If magnetic field is rather a product of decay than dynamo amplification, then the local dimensionless helicity ξ may be close to unity. I cover the range $\xi_\infty = 0.001 \div 0.5$ in simulations to determine the possible dynamical significance of non-zero magnetic helicity.

3.2. Transition to rotationally supported flow

Each real astrophysical accretion flow has non-zero specific angular momentum

$$l = \lambda r_{\rm g} c, \quad \text{or equivalently,} \quad l = v_{K\rm cir} r_{\rm cir}, \tag{57}$$

where $r_{\rm cir}$ is a radius where matter becomes rotationally supported and $v_{K\rm cir}$ is Keplerian velocity at $r_{\rm cir}$. General Newtonian expression for Keplerian velocity at radius r is

$$v_K = c\sqrt{\frac{r_{\rm g}}{2r}}. \tag{58}$$

For larger radii $r > r_{\rm cir}$ angular momentum exerts relatively small force $F_l \sim l^2/r^3$ on plasma, since F_l decreases with radius faster than gravitational force $F_{\rm g} \sim r_{\rm g} c/r^2$. To be consistent with observations, circularization radius for the Galactic center should lie within $r_{\rm cir} = 2r_{\rm g} \div 10^4 r_{\rm g}$. Numerical simulations (Cuadra et al. 2006) suggest $r_{\rm cir} \sim 3 \cdot 10^3 r_{\rm g}$.

Solution with certain $\dot{M}$ is valid if it exists from outer boundary at r_x down to $r_{\rm cir}$. The system of equations (53) has the same properties as spherically symmetric system of hydrodynamic equations (Bondi 1952): subsonic solution exists for all $\dot{M}$ up to maximum $\dot{M}^*$, transonic

solution is valid for the only value $\dot{M}^*$ and no solution exists for $\dot{M} > \dot{M}^*$. The solution with

$$\dot{M} = \dot{M}^*(\text{for transonic solution}) \tag{59}$$

is preferable, because it has the highest rate of energy transfer towards the equilibrium state of the system matter-SMBH. The same argument is valid for a general hydrodynamic nozzle (Landau & Lifshitz 1987). It is reasonable to expect that maximum mass flux solution for system with magnetic field (53) also obeys the condition (59). However, even small amount of angular momentum can change the picture.

When $\lambda \gg 1$, the specific angular momentum (57) of the flow should be able to travel outward through the outer quasi-spherical solution by means of $r\phi$ component of Maxwell stress tensor $t_{\alpha\beta}$. The angular averaged form of this component is

$$t_{r\phi} = \frac{< B_r B_\perp >_\Omega}{4\pi}. \tag{60a}$$

It can be transformed with the aid of Schwartz formula $< xy > \leq \sqrt{< x^2 >}\sqrt{< y^2 >}$ into inequality

$$t_{r\phi} \leq \frac{B_r B_\perp}{4\pi} \tag{60b}$$

with definitions (22) of B_r and $B_\perp$.

Let us take a disk (Shakura & Sunyaev 1973) with height H and write the angular momentum transfer equation as

$$\frac{d(r^2 H t_{r\phi})}{dr} = 0. \tag{61a}$$

The result of integration is (Gammie & Popham 1998)

$$\dot{M} l = 4\pi H r^2 t_{r\phi}, \tag{61b}$$

in case of large dimensionless angular momentum $\lambda \gg 1$ (Gammie & Popham 1998). I take specific angular momentum l from (57) and the accretion rate to be

$$\dot{M} = 2\pi r H \rho v. \tag{62}$$

I substitute angular momentum l from (57), accretion rate $\dot{M}$ from (62), Alfven speeds from definitions (24), Keplerian velocity from (58) and inequality for $t_{r\phi}$ from (60b) into angular momentum transfer equation (61b) to obtain

$$\frac{v v_K}{v_A v_{A\perp}} \sqrt{\frac{r_{\rm circ}}{r}} = 2\alpha, \qquad \alpha \leq 1 \tag{63a}$$

that should be valid at any radius r. This inequality is usually valid for $r > r_{\rm cir}$ if it is valid at $r_{\rm cir}$, so that (63a) can be simplified to

$$\frac{v v_K}{v_A v_{A\perp}} \leq 2 \quad \text{at} \quad r_{\rm cir}. \tag{63b}$$

Condition (63b) can be used when the right-hand side of (63a) decreases more slowly than the square root of radius as r decreases. Height of the disk H cancels out of final expression, thus conditions (63) are approximately valid even for flows with $H \approx r$. Such flows are likely to describe the realistic transition region from outer quasi-spherical inflow to inner rotational solution. I do not have any extra conditions that could appear on the surface of compact object, so I consider object to be a black hole.

As the results of numerical solution of (53) indicate, condition of angular momentum transport (63) may be stronger than maximum accretion rate condition (59) dependent on the value of specific angular momentum l. Two types of solutions are possible:

- maximum accretion rate solutions that describe radial flows with small angular momentum $l < cr_{\rm g}$ (subsection 4.1)
- flows with the effective angular momentum transfer that work for large angular momentum $l > cr_{\rm g}$ (subsection 4.2).

4. Results

4.1. Maximum rate solution

Let me first disregard the angular momentum transport condition (63) and calculate the flow with small angular momentum $l \ll r_g c$, when mean rotation is not dynamically important.

The system of equations I solve (53) can be rewritten as

$$\frac{(F_i)'_r}{F_i} = \frac{N_i(\vec{F}, r)}{D} \quad \text{for} \quad i = 1..8. \tag{64}$$

Here $F_i(r)$ are 8 functions I solve for, $N_i(\vec{F}, r)$ are function- and radius- dependent numerators and

$$D = 1 - \frac{v^2}{V_s^2} \tag{65}$$

is a common denominator. Critical velocity V is

$$V_s^2 = c_{sg}^2 + 2v_{A\perp}^2 \quad \text{with} \quad c_{sg}^2 = c_s^2 + \frac{5u^2}{3}. \tag{66}$$

Effective sound speed c_{sg} is equal to that of plasma with effective particles velocity $v_{pg}^2 = v_p^2 + u^2$.

According to the condition (59) I search for a smooth solution that has a sonic point at some radius r_s. The condition at r_s is $D(r_s) = 0$. Zero denominator requires all the numerators $N_i(\vec{F}, r)$ to be zero at r_s. It can be shown from (53) that all eight conditions $N_i(\vec{F}(r_s), r_s) = 0$ collapse into just one. This fact strengthen the belief that maximum accretion rate solution is transonic.

Two equalities

$$D(r_s) = 0 \quad \text{and} \quad N_1(\vec{F}(r_s), r_s) = 0 \tag{67}$$

give the missing 8-th condition on $\dot{M}$ for (53) and the sonic radius r_s. Thus, I have 7 conditions at the boundary at $3r_B$ and 1 condition somewhere in the region. I employ the shooting method to search for $\dot{M}$ and r_s that satisfy (67).

I obtain the Bondi hydrodynamic model (Bondi 1952), if I set all Alfven velocities and turbulent velocity to zero and use non-relativistic prescription for gas enthalpy w_{gNR} (53c). Therefore, the accretion rate $\dot{M}$ equals Bondi accretion rate for monatomic gas

$$\dot{M}_B = \frac{\pi}{4} r_{\rm g}^2 c^4 \rho_\infty \left(\frac{3\mu}{5RT_\infty} \right)^{3/2} \approx 4 \cdot 10^{-6} M_\odot \text{year}^{-1} \tag{68}$$

in the limiting case of no turbulence. The number is for the Black Hole in our Galactic Center with $r_{\rm g} = 1.1 \cdot 10^{12}$cm (Ghez et al. 2003), $T = 1.5 \cdot 10^7$K and $n \approx 48\text{cm}^{-3}$ (Baganoff et al. 2003). Accretion rate $\dot{M}$ appears to be lower than $\dot{M}_B$ when turbulent energy is non-zero Fig3.

Inhibition of accretion by turbulence has the following explanation. First, energy of magnetic field increases inwards, therefore it exerts back-reaction force stopping matter (Schwartzman 1971). Second, magnetic field serves a very effective mechanism of energy conversion from gravitational to thermal via dissipation of turbulence (Igumenshchev & Narayan 2002). Larger thermal energy causes larger gas pressure that also stops matter. By means of described I can estimate the actual decrease of accretion rate $\dot{M}$ from Bondi value $\dot{M}_B$.

I take my reference model to have the values $\gamma = 1$, $\sigma_\infty = 1$, $\xi_\infty = 0.025$ of, correspondingly, dimensionless scale of turbulence, outer magnetization and outer magnetic helicity. The accretion rates are $0.14\dot{M}_B$ for non-relativistic equation of state and $0.24\dot{M}_B$ for relativistic equation of state. I can now consider the whole ranges of all three parameters and explain the observed correlations between them and accretion rate $\dot{M}$.

Larger flow magnetization σ obviously results in lower accretion rate $\dot{M}$. Larger magnetic field and turbulent velocity field exerts larger back-reaction force on matter. Also, transformation of gravitational energy into thermal happens more readily if magnetization is larger. Larger thermal energy means larger gas pressure and larger back-reaction force on matter striving to fall onto the central object.

Several factors lead to higher magnetization. Obviously, larger outer magnetization σ_∞ makes magnetization in the entire flow σ larger. Then larger dissipation length scale λ inhibits dissipation of magnetic field. Larger magnetic helicity also lowers magnetic energy dissipation and leads to larger magnetization σ. These correlations can be easily observed on Fig3. Increase of the relative length scale of energy containing eddies γ from 0.2 to 2 results Fig3a in about 2 times drop in accretion rate $\dot{M}$. Accretion rate stays constant Fig3b at small values of outer magnetic helicity ξ_∞. However, $\dot{M}$ drops an order of magnitude as turbulence approaches highly helical state at outer boundary $3r_B$ with ξ_∞ close to 0.5. The dependence of $\dot{M}$ on outer magnetization σ_∞ is not quite steep: accretion rate gradually decreases about 4 times as outer magnetization increases 3 orders of magnitude from 0.001 to 1. Surprisingly, accretion rate does

not raise to $\dot{M}_B$ Fig3c even for very small outer magnetization s$\sigma_\infty \sim 0.001$ for non-relativistic equation of state. Even small outer magnetic field increases to smaller radius and influences flow dynamics.

Accretion rate is systematically about 40% higher Fig3 for relativistic equation of state (green line) compared to non-relativistic equation of state (red line). This is because magnetized system has some properties of a non-magnetized one. Formula for Bondi mass accretion rate (68) is valid only for non-relativistic monatomic gas that has an adiabatic index $\Gamma = 5/3$. Accretion rate is higher for higher c and is about 3 times larger (Shapiro & Teukolsky 1983) in case of ultrarelativistic particles with adiabatic index $\Gamma = 4/3$. Accretion rate $\dot{M}$ is determined by (67) at a sonic radius r_s that is smaller than $10^3 r_{\rm g}$ (see Fig3d). Electrons become relativistic at somewhat larger radius about $10^3 r_{\rm g}$ in the solutions of (53). This leads to gas adiabatic index Γ lower than 5/3 at sonic point $r = r_s$. Thus accretion rate is considerably larger in case of relativistic equation of state.

It is also instructive to trace the dependence of sonic radius r_s on parameters. Sonic radius for hydrodynamic accretion of non-relativistic monatomic gas is equal to several Schwarzschild radii $r_s = 2 \div 10 r_g$ (Beskin & Pidoprygora 1995). Sonic radius is a considerable fraction of r_B for a gas with adiabatic index Γ substantially smaller than 5/3 for non-magnetized accretion (Bondi 1952). Magnetized accretion has the same properties. Non-relativistic EOS (green line) results in very small sonic radius $r_s = 7 \div 11 r_{\rm g}$ Fig3d. Sonic radius for relativistic EOS (red line) is $r_s = 300 \div 1200 r_{\rm g}$ about the radius where electrons become relativistic $r \sim 10^3 r_{\rm g}$. The value of sonic radius drops several times as plasma outer magnetization σ_∞ increases from 0.001 to 1. As outer magnetization σ_∞ increases, accretion rate drops Fig3c, because density ρ and gas inflow speed v decrease. Equality of sonic speed V_s and inflow speed v occurs closer to the black hole as σ_∞ increases because of decrease of v.

Inflow velocity v as well as other characteristic velocities of the flow are depicted on Fig4 as functions of radius r for the reference model with $\sigma_\infty = 1$, $\gamma = 1$, $\xi_\infty = 0.025$. All velocities are normalized to free-fall speed

$$v_{ff} = c\sqrt{\frac{r_{\rm g}}{r - r_{\rm g}}}. \tag{69}$$

I also normalize perpendicular Alfven velocity $v_{A\perp}$ and turbulent speed u to one dimension. Horizontal line on Fig4 corresponds to radial dependence $r^{-1/2}$.

Inflow velocity v (red) monotonically increases inwards, whereas sound speed c_s (green) monotonically decreases with intersection almost at sonic point. Radial Alfven velocity (grey) v_{Ar}, perpendicular Alfven velocity $v_{A\perp}$ (orange) and turbulent velocity u (blue) Fig4 start out as constants from outer boundary at $3r_B$, where turbulence is sustained by external pumping. Then these velocities increase and deviate from one another. Radial Alfven velocity v_{Ar} appears to be much higher than $v_{A\perp}$ and u in the inner accretion region. This fulfills the expectations of earlier models (Shakura & Sunyaev 1973), (Scharlemann 1983), (Beskin & Karpov 2005). At small radius turbulence is driven by freezing-in amplification of magnetic field and random velocity. Left-hand sides of turbulence evolution equations (53d), (53e) and (53f) dominate over corresponding terms with external driving for radius $r \lesssim 10^4 r_{\rm g}$. Internal driving of v_{Ar} is

much more effective than driving of $v_{A\perp}$ and u. Therefore radial Alfven velocity v_{Ar} is larger than other two speeds. This refutes any model with isotropic magnetic field.

Several pairs of lines intersect on velocity plot Fig4. I consider three main intersection points for the reference model with $\sigma_\infty = 1$, $\gamma = 1$, $\xi_\infty = 0.025$ and relativistic EOS (Fig4a). Crossing of inflow velocity v (red) and sound speed c_s (green) occurs almost at sonic point r_s, determined by (67) with critical velocity V_s (66). No plasma waves can escape the region with large inflow velocity $v > V_s$. Approximately $c_s \approx V_s$ at sonic point $r_s \approx 6 \cdot 10^{-4} r_B$, because of low magnetization $\sigma \approx 20\%$ in that region Fig5a. Alfven point is determined by equality $v = v_{Ar}$ at radius r_A. Alfven waves cannot escape from the region where inflow speed is greater than radial Alfven speed v_{Ar}. Equality holds at relatively large radius $r_A \approx 0.03 r_B$. The third combination of the same three velocities also gives a characteristic intersection point. Radial Alfven speed v_{Ar} increases faster inwards and becomes equal to sound speed c_s at about $r \approx 4 r_g$. Further relative increase of v_{Ar} leads to magnetic energy dominated flow what can be traced on magnetization plot Fig5a.

Fig5a shows evolution of plasma magnetization σ with radius r for the reference model. Clearly, thermal energy equipartition assumption does not hold, id est turbulent energy does not equal to constant fraction of thermal energy $\sigma \neq$ const. Magnetization σ varies more than one order in magnitude from 0.07 to 3. It starts out at initial $\sigma_\infty = 1$ at $3 r_B$, where turbulence is supported by external energy input $Q_+ =$ const. Then σ deviates down as r decreases. Magnetization σ drops, because length scale L decreases with radius r that causes turbulence to decay faster. At about $0.03 r_B$ magnetization starts to rise as internal turbulence driving takes over. Inflow velocity v slightly deviates up from Alfven velocity v_A as r decreases. Since internal driving rate is proportional to v (left-hand sides of (53d), (53e) and (53f)) dissipation rate is proportional v_{Ar}, parameter σ grows slightly with decreasing radius. The growth is about a factor of 5 for 3.5 orders of magnitude decrease in radius. Magnetization σ jumps up in the region very close to the event horizon of the black hole. However, this jump may originate from inconsistent treatment of General Relativity.

The dependence of magnetic helicity ξ with radius is shown on Fig5b. The curve for ξ behaves like the inverse of magnetization curve for magnetization σ Fig5a. Such a behavior can be easily seen from the magnetic helicity equation (53g). Magnetization σ decreases order of magnitude during the transition from externally supported to internally supported turbulence around $r \approx 0.03 r_B$. The same order of magnitude from 0.025 to 0.2 increases magnetic helicity ξ. Then ξ gradually decreases down to initial value. Thus magnetic helicity ξ does not change dynamics if it is initially small $\xi_\infty \lesssim 0.1$. Only when ξ_∞ is large, accretion rate drops.

Deviation of inflow velocity v from free-fall scaling $r^{-1/2}$ makes a density profile in magnetized flow different from standard Advection Dominated Accretion Flow (ADAF). Despite I consider the flow where energy is only advected inwards, I obtain

$$\rho \propto r^{-\zeta} \quad \text{with} \quad \zeta \approx 1.25 \tag{70}$$

almost independently on the outer parameters or the equation of state, somewhat shallower than $\rho \propto r^{-1.5}$ in ADAF.

The only question left is how well this flow with maximum accretion rate can describe the real situation with large angular momentum l. Given the solution of the system (53) I can check whether the condition for effective angular momentum transport (63) holds. The ratio of velocities in (63) appears to be larger than the right-hand side for circularization radius $r_{\rm cir} > r_{\rm g}$ for the parameters ξ_∞, σ_∞ and γ within the chosen range. This makes a flow with maximum accretion rate unable to effectively transport the angular momentum outwards. The same conclusion can be made simpler. The transport of angular momentum is a magnetic process. So, l can be transported only with the speed of bending magnetic field lines that is Alfven speed. However, Alfven waves cannot escape from the region within $r_A \approx 0.03 r_B$ from the compact object that makes angular momentum transport impossible even from quite large radius.

4.2. Solution with effective angular momentum transport

Solution with large outer angular momentum has properties, substantially different from those of maximum-rate solution. The actual details of solution and allowed accretion rate depend on how this angular momentum is transported. For the simple estimate I suppose that the accretion rate is determined by the equality in angular momentum transport condition (63). Maximum accretion rate $\dot{M}$ for (63) appears to be about two orders of magnitude lower than Bondi rate $\dot{M}_B$ (68).

I add one parameter to the reference model: unknown circularization radius $r_{\rm cir}$ for specific angular momentum l (57). I take it to be $r_{\rm cir} = 10^3 r_{\rm g}$ for the reference model. Plots of the accretion rate verses model parameters are shown on Fig. 6. Dependencies for rotating solution Fig6 have the opposite slopes to those for the maximum-rate solution Fig3. Accretion rate $\dot{M}$ increases with increasing outer magnetization σ_∞ Fig6b and increasing outer magnetic helicity ξ_∞ Fig6c. Both effects lead to higher plasma magnetization σ. I explained in the previous subsection 4.1 that magnetic field plays an inhibiting role on matter inflow and the larger the magnetic field, the smaller the accretion rate $\dot{M}$ is. However, the different effect takes over in case of rotating flow.

The allowed in condition (63) inflow speed v is proportional to the product of radial Alfven speed v_{Ar} and perpendicular Alfven speed $v_{A\perp}$. Larger magnetic field results in larger transport of angular momentum outward, so larger inflow velocity v and larger accretion rate are possible. Larger outer magnetization σ_∞ and larger outer magnetic helicity both lead to higher magnetization σ and higher magnetic field. Inhibiting effect of magnetic field is smaller in case of lower accretion rates $\dot{M}$ and lower inflow velocities v. Lower v results in lower relative driving of turbulence that makes magnetic field weaker. Weaker magnetic field has weaker influence on dynamics. So larger magnetic field B results in larger accretion rate $\dot{M}$, when it needs to transfer angular momentum.

The dependence of $\dot{M}$ on length scale γ is obscured by the dependence of external driving on γ. Accretion rate $\dot{M}$ is smaller for smaller magnetic field, but the state of low magnetization

can be achieved in two different ways. Firstly, Magnetic field decays faster when L decreases. However, the plasma at circularization radius $r_{\rm cir} = 10^3 r_{\rm g}$ is still partially influenced by the outer boundary conditions. Internal driving does not depend on L, whereas external driving is stronger and magnetization σ is higher, when L is small. The described two effects balance each other and make accretion rate $\dot{M}$ almost independent of dimensionless length scale γ Fig6a.

Accretion rate $\dot{M}$ decreases with decrease of circularization radius $r_{\rm cir}$ Fig6d for non-relativistic equation of state. To explain this, I trace on Fig7b all the quantities that enter angular momentum transport condition (63b) for the reference model. Fig7b shows velocities normalized with the free-fall speed (69). Keplerian velocity v_K is constant in these coordinates by definition (58) as long as $r \gg r_{\rm g}$. Inflow speed v (red line) and radial Alfven velocity v_{Ar} (grey line) reach constant value at about $0.02 r_B$. The only changing quantity for $r < 0.02 r_B$ is perpendicular Alfven velocity $v_{A\perp}$ (orange). Because $v_{A\perp}$ decreases with radius, the allowed v and $\dot{M}$ are smaller for smaller circularization radius.

However, accretion rate increases for small circularization radii for 1-T equation of state Fig.6d (green line). This is the consequence of the increasing gas heat capacity, when electrons reach relativistic temperatures. Higher heat capacity solutions are known to have larger accretion rates (Bondi 1952) that is equivalent to the lower inflow speeds v in the solutions for the fixed matter inflow rate. Velocity v (Fig7a (red line)) starts deviating down from the self-similar solution at approximately $10^3 r_{\rm g}$, making the solutions with higher $\dot{M}$ possible. In fact, condition (63) for the solutions with small $r_{\rm cir}$ becomes critical at some fixed point $r_d > r_{\rm cir}$ instead of reaching equality at $r_{\rm cir}$ (63)b. Therefore, according to (63)a, maximum value of the inflow speed grows with the decrease of circularization radius as $v \propto r_{\rm cir}^{-1/2}$, explaining the rise of accretion rate for small $r_{\rm cir}$ (see green curve on Fig.6d) for 1-T equation of state.

Solution for non-relativistic equation of state, in turn, possess its own feature. Self-similar flow Appendix C settles in at $10^3 r_{\rm g}$, making accretion rate almost independent on circularization radius Fig.6d. Magnetic helicity ξ in such a flow is a number about unity that is consistent with self-similar solution C. Self-similar flow can not establish for 1-T equation of state, because relativistic effects become important before it establishes and break self-similarity.

In fact, magnetization σ and magnetic helicity ξ Fig.8 are not constant at small radii for correct 1-T EOS, because these relativistic corrections work. At about $0.01 r_B$ magnetization reaches almost constant level $\sigma \approx 0.02$ Fig8a and then starts to slightly deviate down, because equilibrium σ for the matter with higher heat capacity per particle $c > 3k/2$ is lower. Magnetic helicity ξ behaves Fig8b the opposite to magnetization σ : magnetic helicity reaches $\xi \approx 1.5$ at $0.01 r_B$ and start to slightly deviate up as radius decreases.

5. Discussion of the model

I present the sophisticated analytical model to determine the properties of spherical magnetized accretion. The common assumptions of magnetic field isotropy and thermal equipartition are released, but many assumptions are still left. As usually in fluid dynamics a lot of sim-

plifications are made during the course of elaboration. The validity of almost everything can be questioned. The system of equations (53) may not describe the real flow 5.1 or may have some inaccuracies 5.2. Gas cooling may not be neglected 5.3, 5.4. Convection and diffusion can entirely change the flow (Quataert & Gruzinov 2000). The equation of state was also found to influence the dynamics. Let me discuss all these topics and determine the practical significance of the model.

5.1. Real Flow

Presented model is partially applicable to the real systems. It may describe some gas flows onto Supermassive Black Holes in Low Luminosity Galactic Centers, in particular in the center of our Galaxy. These flows are geometrically thick (Narayan & Yi 1995) and may have low angular momentum (Moscibrodzka, Das, & Czerny 2006). However, the real flows may have properties that my model cannot handle in its current state. First of all, the sources of matter and external driving should be explicitly accounted for. Secondly, the self-consistent angular momentum transport theory is needed.

The material is mainly supplied to the central parsec of the Milky Way by stellar winds (Quataert 2004). The wind-producing stars have a broken power-law distribution as a function of radius (Baganoff et al. 2003). Some stars are as close to the central black hole as $0.1r_B$ (Ghez et al. 2003). The stars supply too much material to be accreted, therefore there exist an outflow (Quataert 2004). Bondi radius coincides with the radius where inflow starts to dominate outflow in numerical simulations with the accretion rate $\dot{M} \sim 10^{-6} M_{\odot}\text{year}^{-1}$ (Cuadra et al. 2006). Maximum accretion rate in the solution with zero angular momentum is $0.2\dot{M}_B \approx 10^{-6} M_{\odot}\text{year}^{-1}$ and $0.01\dot{M}_B$ for the rotating flow. So that the transition from outflow in inflow happens at $r \gtrsim 10^5 r_{\text{g}}$.

I can show that outflows do not change the accretion rate from calculated. Outflows substantially alter the value and the sign of inflow velocity v in the system (53). However, the differences in inflow velocity do not influence any other quantity as long as three conditions are satisfied:

1. v is much smaller than the gas particles velocity v_p, kinetic energy of gas is negligible in the outflow region
2. external driving of turbulence Q_+ dominates over internal driving there
3. condition on $\dot{M}$ is set in the inflow region.

The first two conditions are satisfied down to $r \sim 10^4 r_{\text{g}}$ (see Fig4 and Fig7). The third condition holds for maximum rate solution, because condition on $\dot{M}$ is set at the sonic point $10^3 r_{\text{g}}$ from the central object. It also holds for the solution with angular momentum transport, because the condition on $\dot{M}$ is usually set at the inner boundary $10^3 \div 10^4 r_{\text{g}}$. All three above conditions

holds, hence outflows of stellar winds do not substantially change the accretion rate or any quantity in the system.

Self-consistent calculation of angular momentum transport can lead to a different accretion rate than calculated with (63). Condition for effective angular momentum transport (63) leads to only an order of magnitude estimate of $\dot{M}$. Two concurrent effects can change the accretion rate in the real flow. Firstly, the equality $\alpha = 1$ in (63a) is the extreme regime. Physical flow may have much smaller transport coefficient $\alpha \lesssim 0.1$ that corresponds to more than 10 times smaller $\dot{M}$. However, angular momentum is being transported in the entire flow, not only from circularization radius $r_{\rm cir}$. As matter travels to $r_{\rm cir}$, the amount of specific angular momentum left becomes smaller. If the transport is very effective, matter travels inwards in a spherical accretion (Shakura & Sunyaev 1973). Angular momentum transport may be enhanced by higher magnetic field. There is another source of magnetic field in a rotating flow: MagnitoRotational Instability (MRI) (Hawley & Balbus 2002). I discuss it in the next subsection 5.2.

5.2. Treatment of Magnetic field

The long history of accretion theory has many accepted models based on ideas, extended beyond the area of applicability of these ideas. For example, general relativity was substituted with Paczynski-Wiita gravitational potential (Paczhynski & Wiita 1980), (Shakura & Sunyaev 1973). Magnetic field was long treated similar to the normal matter (Narayan & Yi 1995), (Coker & Melia 2000). Displacement current was neglected in magnetic field dynamics that allowed to treat magnetic field without electric field (Scharlemann 1983). System of viscous equations describe viscosity by a single parameter (Shakura & Sunyaev 1973), (Landau & Lifshitz 1987), (Landau, Lifshitz & Pitaevskii 1984), (Biskamp 2003). Gyrokinetics is used to solve the problems with non-Maxwellian distribution functions (Sharma et al. 2007), power-law non-thermal electrons are usually present in plasma (Yuan et al. 2002). The final solution of accretion problems lies in the domain of plasma physics.

Described above model is extended in several ways, mainly with regard to magnetic field. Isotropic MHD system of turbulent equations (28) describes the real box collisional turbulence quite well, because it corresponds to convergent set of simulations. Collisionality assumes that medium behaves like many particles with short-range interactions. However, astrophysical medium of interest is always collisionless with prevailing long-range interactions. I inconsistently use the results of numerical simulations of collisional MHD (1)-(7) with magnetic resistivity ν_M on the order of viscosity ν, because the realistic simulations of collisionless plasma turbulence are not done by anyone and are unlikely to be done in the near future (Schekochihin et al. 2004).

Observations of astrophysical turbulence may give more information than numerical simulations. A special case of collisionless plasma is plasma with random kinetic energy much smaller than random magnetic energy. This regime is a good picture of Sun corona with all plasma effects come into play (Aschwanden 2005). Dissipation of magnetic loops with low ki-

netic energy proceeds mainly via reconnections. The timescale of reconnective dissipation was found to be

$$\tau_{\rm rec} \approx 20 \frac{L}{v_A} \tag{71}$$

(Noglik, Walsh, & Ireland 2005). The same number was also predicted (Lazarian & Vishniac 1998). Collisional MHD turbulence has much smaller dissipation timescale

$$\tau_{\rm diss} \approx 1 \frac{L}{v_A} \tag{72}$$

(28), (36). Plasma has large kinetic energy in the outer region of accretion flow, where turbulence is externally supported. Timescale $\tau_{\rm diss}$ (72) may be appropriate there. Kinetic energy E_K decreases to smaller radii and magnetization σ increases Fig4 in case of zero angular momentum 4.1. Accretion flow then resembles solar Corona (Aschwanden 2005). Dissipation timescale may increase order of magnitude and be close to $\tau_{\rm rec}$ (71). This increase would lead to much lower accretion rate, because higher magnetic field leads to lower $\dot{M}$. Matter infall may eventually proceed through the regions of lower magnetic fields (Igumenshchev 2006).

Even if I assume that box isotropic turbulence (28) with coefficients (36) is applicable to isotropic turbulence, there are at least four complications in building the full anisotropic theory.

First of all, I needed to introduce arbitrary coefficients c_{uB2}, c_{BB2}, c_{Bu2} to describe isotropization of anisotropic magnetic field and anisotropic energy transfer between magnetic field and fluid motions. These coefficients were taken to be have reasonable values to satisfy rather loose analytical tests (Appendix A). However, changes in these coefficients do not lead to dramatically different accretion rate or flow structure. Setting $c_{BB2} = c_{BB1}$ instead of $c_{BB2} = 0$ leads to only 10% of $\dot{M}$ change for the reference model. All seven introduced coefficients c_{xx} may themselves depend on anisotropy of the magnetic field. The details of anisotropic MHD are still debatable (Goldreich & Sridhar 1995), (Boldyrev 2006). I leave the incorporation of anisotropic MHD model into accretion theory for future work.

Secondly, the presented theory is not generally relativistic. Accretion rate $\dot{M}$ appears to be insensitive to the choice of gravitational potential. The condition on $\dot{M}$ is set at about $10^3 r_{\rm g}$ in case of relativistic EOS and zero l. Sonic point is situated close to the black hole at $r_s = 5 \div 10 r_{\rm g}$ for non-relativistic equation of state. But 1% increase of $\dot{M}$ leads to the sonic point at $r_s > 100 r_{\rm g}$, independent of the way to mimic general relativity. However, the region near the black hole is important, because part of IR radiation as well as part of radio emission comes from several Schwarzschild radii (Narayan et al. 1998), (Falcke & Markoff 2000), (Marrone 2007). Thus, to fully constrain theory by observations general relativity is a must.

In third, magnetic helicity H involves numerous complications. I discuss problems of box helicity in Appendix B. The incorporation of H into accretion flow brings an additional problem. Magnetic helicity evolves in the region that is frozen into matter. The distance $L_{||}$ between radial boundaries of this region is proportional to inflow velocity v, thus $L_{||}$ increases with increasing v and at some point $L_{||} > r$, whereas size in the angular direction is about $L = \gamma r$. A part of the region is getting sucked into the black hole, while a part is still situated at fairly large radius r. Equation of magnetic helicity evolution (53g) holds only if I assume

even redistribution of helicity over the mass of plasma. This holds for frozen magnetic field, but in the reality diffusion and convection are present. Diffusion may change the results for H (53g) as well as for the entire flow pattern. I also leave these uncertainties for future research.

Finally, it was recently suggested (Beskin & Karpov 2005) that ions and electrons should be viewed in accretion as confined by magnetic field lines. This is the opposite of standard picture where magnetic field lines are frozen into matter (Scharlemann 1983). The former case has higher heating rate of matter under contraction (Beskin & Karpov 2005), because of conservation of the first adiabatic invariant $I = 3cp_t^2/(2eB) = \text{const}$ (Landau & Lifshitz 1971). Here p_t is a particles momentum in the direction perpendicular to $\vec{B}$. However, only highly magnetized flows with magnetization $\sigma > 1$ conserve I. Non-linear interactions of particles in low-σ plasma are likely to isotropize the distribution of particles. When particles are heated isotropically under contraction, general Magneto-Hydrodynamics (1)-(7) works (Landau, Lifshitz & Pitaevskii 1984) and heating rate stays unchanged. Magnetization in computed models is below unity Fig5a and Fig8a. Thus the application of first adiabatic invariant conservation to magnetized accretion flow seems irrelevant.

Mean rotation of the flow also creates anisotropy. Because inner gas rotates faster than outer, Magneto-Rotational Instability (MRI) works. It produces the additional driving of magnetic field that may be concurrent to other sources. Magneto Rotational Instability (Hawley & Balbus 2002) has a timescale

$$\tau_{MRI} = -\left(r\frac{d(l/r^2)}{dr}\right)^{-1}. \tag{73}$$

When MRI timescale becomes larger then dynamic timescale $\tau_{\rm dyn} = r/v$, field amplification occurs mainly because of regular tangential motion, instead of regular radial motion. MRI may be crucial even in the region without rotational support. Full consideration of effects of angular momentum on the flow is the subject of the next study.

5.3. Radiative cooling

The system of equations (53) describes the accretion flow, where all the energy is stored in the same piece of matter where it initially was. There is no energy loss by diffusive or radiative cooling.

Let me estimate the radiative cooling first. Line cooling is more effective than bremsstrahlung cooling for temperatures about $T_\infty \approx 1.5{\cdot}10^7 K$. Line cooling function is $\Lambda \approx 6{\cdot}10^{-23} n^2 (T/10^7 K)^{-0.7}$erg cm^{-3}s^{-1} (Sutherland & Dopita 1993). Thus characteristic cooling time $\tau_{\rm cool}$ is

$$\tau_{\rm cool} = \frac{3RT\rho}{2\Lambda\mu} \approx 1\cdot 10^{12}\text{s} \tag{74}$$

for our Galactic Center accretion. The dynamic timescale $\tau_{\rm dyn} = r/v$ for accretion with rate $\dot{M} = 0.1\dot{M}_B$ (68) is

$$\tau_{\rm dyn} = \frac{\rho r^3}{\dot{M}} \approx 5\cdot 10^{10}\text{s} \tag{75}$$

with continuity equation (10) at radius $r = r_B$ (55). Cooling time is about 20 times larger than inflow time in the region where outflows dominate. Nevertheless, anisotropy of stellar winds may lead to significant cooling of some clumps of matter (Cuadra et al. 2005). Even the disk may form (Cuadra et al. 2006). Careful calculation with line cooling is yet to be done.

5.4. Convection & Diffusion

The system (53) does not include diffusive processes or convection. Thus I have Advection-Dominated flow despite magnetic field and matter can exchange energy between each other. This approach is not self-consistent. Viscosity is responsible for turbulence dissipation, but the same viscosity should be accounted for in diffusion parts in the equations of presented system (53). Momentum, energy, angular momentum, magnetic field, magnetic helicity should all diffuse. However, self-consistent consideration of diffusive terms makes system of equation second order in coordinate. This requires other solution techniques. That is why the second order diffusion terms are often omitted.

Transport of quantities may substantially increase if convection is present. The presence of diffusion smears out all small scale perturbations, so high-frequency stability criteria (Scharlemann 1983) are inapplicable. Exchange of large blobs should be calculated instead AppendixD. Described magnetized accretion flows are convectively stable on average, but some other instabilities may lead to weak convection AppendixD. However, power of diffusive energy transfer is not affected. Strong diffusion can only be slightly enhanced by weak convection. Self-consistent calculation of diffusive processes and the exact balance between convection and diffusion is the subject of the future study.

5.5. Equation of state

The difference in accretion rate $\dot{M}$ between one-temperature relativistic and 1-T non-relativistic EOSs is up to 40% for maximum rate solution 4.1 and up to several times for solution with effective angular momentum transport 4.2. Solution with smaller gas adiabatic index Γ has larger accretion rate $\dot{M}$ (Shapiro & Teukolsky 1983). Adiabatic index gradually falls from $\Gamma = 5/3$ to $\Gamma = 1.43$ in case of relativistic EOS as matter approaches the black hole.

However, the electron temperature T_e is unlikely to be equal to ion temperature T_i. Electron temperature T_e is usually modelled to be lower than T_i (Narayan & Yi 1995). This two-temperature model has lower gas pressure support and larger gas adiabatic index Γ than 1-T model with $T = T_i$. Lower gas pressure itself leads to higher accretion rate, larger Γ itself leads to lower accretion rate. The combination of these two effects is expected to change the accretion rate by about the same factor as present between relativistic and non-relativistic 1-T EOSs. The exact details depend on the two-temperature model chosen.

6. Observations

Proposed quasi-spherical magnetized accretion model is aimed to explain plasma flow onto Super-Massive Black Hole Sgr A* in our Galactic Center. Many observations of this source are done. These observations reasonably agree with the results of my model.

A common misconception about Chandra X-Ray observations of Sgr A* exists in literature. X-Rays mainly originate in the region that lies further than Bondi radius r_B from the central object. Thus characteristic density ρ_∞ and temperature T_∞ far from the Black Hole can be found (Baganoff et al. 2003). If one knows the mass M, this automatically gives Bondi accretion rate $\dot{M}_B$ (68). However, accretion rate is not necessarily determined by this formula (68), unlike some papers suggest (Bower et al. 2005). In my model accretion rate $\dot{M}$ is independent on radius and is smaller than $\dot{M}_B$.

IR (Eckart et al. 2006) and Radio (Zhi-Qiang Shen 2006) observations are difficult to interpret, because they dependent strongly on the accretion model. Density of matter ρ is better related to observations than accretion rate $\dot{M}$. The general agreement is (Yuan et al. 2002) that density ρ should be lower than in Bondi solution ρ_B in the region close to the black hole. Solutions with outflows (Yuan, Quataert, & Narayan 2003) and Convectively-Dominated flows (Quataert & Gruzinov 2000) were invented to explain this lower density. Magnetized solution without angular momentum does well the same job. Let me consider two models: (A) with outer magnetization $\sigma_\infty = 0.001$ and (B) with $\sigma_\infty = 1$. The rest of the parameters are: $\gamma = 1$, $\xi_\infty = 0.025$, $l = 0$, 1-T relativistic equation of state. The ratio of densities is

$$\frac{\rho_B}{\rho_A} \approx 0.27 \quad \text{at} \quad 10 r_{\rm g}. \tag{76}$$

Density in magnetized model is much lower than in non-magnetized one. Also, the magnetization at $10r_{\rm g}$ is about $\sigma \approx 0.5$ for B model, that is lower than equipartition. The combination of lower density $\rho < \rho_B$ and subequipartition magnetic field $\sigma < 1$ qualitatively agrees with found small Faraday rotation measure (Marrone 2007). Thorough comparison of radiation in my models with observations is the subject of the future study.

7. Conclusions

Though many ways of dealing with inefficient accretion were invented, my approach is substantially different from all previous efforts. **I elaborated the model that**

- has very few free parameters,
- self-consistently includes averaged turbulence, combining geometrical effects of freezing-in amplification with dissipation,
- ties evolution of random magnetic field and random velocity field to numerical simulations,
- connects outer externally supported turbulence to inner self-sustained turbulence,

- predicts the accretion rates $\dot{M}$ and flow patterns for the flows with negligible angular momentum,
- gives the order of magnitude estimate of $\dot{M}$ for large angular momentum flows.

The model predicts

- accretion rate $\dot{M}$ of magnetized fluid $0.2 \div 0.7$ of Bondi rate $\dot{M}_B$ even for small outer magnetization σ_∞,
- subequipartition magnetic field in the outer part of the flow and superequipartition in the inner part,
- several times lower density than in Bondi model near the central object, what helps to explain observations,
- half an order of magnitude effect of different equations of state on the accretion rate,
- unimportance of magnetic helicity conservation,
- ineffectiveness of convection. Convection and diffusion should be accounted for together.

The next version of the model will include

- more anisotropic effects, in particular, magneto-rotational instability,
- two-temperature equations of state,
- full treatment of angular momentum transport,
- diffusion of momentum, heat and magnetic field.

8. Acknowledgements

The author is grateful to Ramesh Narayan for fruitful discussions. The author thanks Pascal Demoulin for useful comments about magnetic helicity and Ya. N. Istomin for general comments. This work in not supported by any grant.

A. Analytical tests

Let me consider my model in anisotropic incompressible case of box turbulence. Again, I substitute $d/dt = -v\partial/\partial r$ in (23), (25), (27) and set $r = \text{const}$. The box has infinite volume. I express some of unknown c_{xx} in terms of known $\hat{c}_{xx}$ from (29). The system now reads

$$\frac{d(v_{Ar}^2)}{dt} = \frac{(\hat{c}_{Bu} v_{Ar}^2 + 2c_{Bu2}(v_{A\perp} - v_{Ar})v_{Ar})u - (\sqrt{3}\hat{c}_{BB} v_{Ar} + 2c_{BB2}(v_{A\perp} - v_{Ar}))v_{Ar}^2}{L}, \quad \text{(A1a)}$$

$$\frac{d(v_{A\perp}^2)}{dt} = \frac{(\hat{c}_{Bu} v_{A\perp}^2 + c_{Bu2}(v_{Ar} - v_{A\perp})v_{A\perp})u - (\sqrt{3}\hat{c}_{BB} v_{A\perp} + c_{BB2}(v_{Ar} - v_{A\perp}))v_{A\perp}^2}{L}, \quad \text{(A1b)}$$

$$\frac{d(u^2)}{dt} = \frac{(\hat{c}_{uB}(v_{Ar}^2 + 2v_{A\perp}^2) - c_{uB2}(v_{Ar} - v_{A\perp})^2)u - c_{uu}u^3}{L}. \quad \text{(A1c)}$$

I need to determine two coefficients c_{uB2} and c_{Bu2} and prove the entire system (A1) makes sense.

There are three kinds of analytical tests divided by the degree of their certainty. The tests from the first group have solid physical grounds. The tests from the second group represent how turbulence is believed to work, these are the general relations with clear physical insight. The third group of tests consists of the order of magnitude relations and the disputable ideas.

The tests of the first group are proven to work. Only one test of this kind can be applied to our system. This is the energy decay test. Free incompressible MHD turbulence has decreasing with time total energy, because energy decrease corresponds to the increase of entropy of the system gas/magnetic field (Landau, Lifshitz & Pitaevskii 1984).

$$\frac{d}{dt}\left(\frac{v_{Ar}^2 + 2v_{A\perp}^2 + u^2}{2}\right) < 0 \quad \text{for at least one of} \quad v_{Ar}, v_{A\perp}, u \quad \text{non-zero.} \quad \text{(A2)}$$

I take sum with proper coefficients of the right-hand sides of (A1). Then I maximize it with respect to $v_{A\perp}/v_{Ar}$ and v_A/u. I find that when

$$2c_{Bu2} + c_{uB2} \gtrapprox -2.2, \quad \text{(A3)}$$

total energy decreases with time for any non-zero v_{Ar}, $v_{A\perp}$ and u. Let me remind the reader that all these velocity are non-negative according to definitions (24). Condition (A3) is weak. Some tests from the second and the third categories constrain c_{uB2} and c_{Bu2} better, thus making (A3) valid.

The typical test of the second category deals with dynamo amplification of anisotropic field. Dynamo action not only amplifies magnetic field, but also isotropizes it. I take isotropization condition to be

$$\frac{d(v_{Ar} - v_{A\perp})}{dt(v_{Ar} - v_{A\perp})} \leqslant 0. \quad \text{(A4)}$$

Taking expressions for derivatives from (A1) I arrive at

$$(\hat{c}_{Bu} - 3c_{Bu2})u - \sqrt{3}c_{BB2}(v_{Ar} + v_{A\perp}) + c_{BB2}(2v_{Ar} + v_{A\perp}) \leqslant 0 \quad \text{(A5a)}$$

This condition should hold when any speed is much larger then two others. Therefore, (A5a) is equivalent to

$$c_{\hat{Bu}} < 3c_{Bu2}, \qquad c_{BB2} < \frac{\sqrt{3}}{2}\hat{c}_{BB}. \quad \text{(A5b)}$$

Another second category dynamo test states that magnetic field should always increase in some direction if dynamo operates without dissipation. This occurs when Alfven speeds are much smaller than turbulent velocity field. Positive amplification condition then reads

$$\frac{dv_{Ar}^2}{dt \cdot v_{Ar}^2} > 0, \qquad \frac{dv_{A\perp}^2}{dt \cdot v_{A\perp}^2} > 0. \tag{A6}$$

Taking the expressions for derivatives from (A1) and applying the limit $v_{Ar} \ll u$ and $v_{A\perp} \ll u$ I obtain that (A6) is valid for any balance between v_{Ar} and $v_{A\perp}$ when

$$\hat{c}_{Bu} > 2c_{Bu2}. \tag{A7}$$

Inequalities (A5b) and (A7) give tight constrains on c_{Bu2}.

The similar test exists for the random velocity. Magnetic field is supposed to increase the turbulent velocity in the limit $v_{Ar} \sim v_{A\perp} \gg u$. The correspondent condition

$$\frac{d}{dt}\left(\frac{u^2}{2}\right) > 0 \quad \text{for} \qquad v_{Ar} \sim v_{A\perp} \gg u \tag{A8}$$

reduces for (A1) to the condition of constant positive acceleration that initially steady magnetic field applies to matter. Finally

$$c_{uB2} < \hat{c}_{uB}. \tag{A9}$$

MHD decay test of the second kind makes a statement about the balance between random velocity field and magnetic field when the latter is isotropic on average. Numerical simulations show equality of magnetic field dissipation rate and random velocity dissipation rate (34) when initial magnetic energy equals initial kinetic energy. However, this equality should be stable, otherwise kinetic and magnetic energy would diverge from each other after any perturbation and equality of u and v_A would not have been observed. Stability condition is

$$\frac{d(v_{Ar}^2 + 2v_{A\perp}^2 - u^2)}{dt \cdot (v_{Ar}^2 + 2v_{A\perp} - u^2)} < 0 \tag{A10}$$

for $v_{Ar} = v_{A\perp} = u$. Inequality holds for coefficients (36).

The are no more proven or justified assumptions I can make. However, I still need to convert inequalities (A3), (A5b), (A7) and (A9) into equalities applying unjustified tests of third category. I take the value of c_{Bu2} in the middle of the allowed interval

$$c_{Bu2} = \frac{1}{2}\left(\frac{1}{2} + \frac{1}{3}\right)\hat{c}_{Bu} \approx 0.29. \tag{A11}$$

The value of c_{uB} is small compared to the values of other coefficients. There is no physical sense in the sharp increase of u^2 build-up when magnetic field becomes anisotropic that would be the case for $c_{uB2} \ll (-\hat{c}_{uB})$ Turbulent velocity may be expected to increase regardless of the direction of magnetic field in (A1c). This idea leads to $|c_{uB2}| < \hat{c}_{uB}$. I take

$$c_{uB2} = 0 \tag{A12}$$

for the simple estimate. Similar estimate allows me to set

$$c_{BB2} = 0. \tag{A13}$$

In this case isotropization of magnetic field has a timescale about the dissipation timescale.

B. Magnetic helicity conservation from flux tubes

Magnetic helicity in the form (38) is difficult to apply to analytic theory. Another form of this complexity measure of magnetic field may be utilized instead. I believe that magnetic helicity can be well approximated by self-helicity of twisted large loops or flux tubes of size L (this is the subject of a future paper). Sample loops are depicted on Fig.1. Expression for magnetic helicity is now

$$H = n \cdot N\Phi^2, \tag{B1}$$

where $n \gtrsim 1$ is a number of flux tubes in the region of interest, N is the number of windings of magnetic field lines around the flux tubes tori, Φ is magnetic flux in flux tube. Number of windings N_i of each tube is either positive (+) or negative (-) depending on whether field lines are winded clockwise (+) or counterclockwise (-) around the tube's mean field. Both flux tubes on Fig. 1 have negative N_i. I define N as an absolute value of an average

$$N = \frac{|\sum N_i|}{n}. \tag{B2}$$

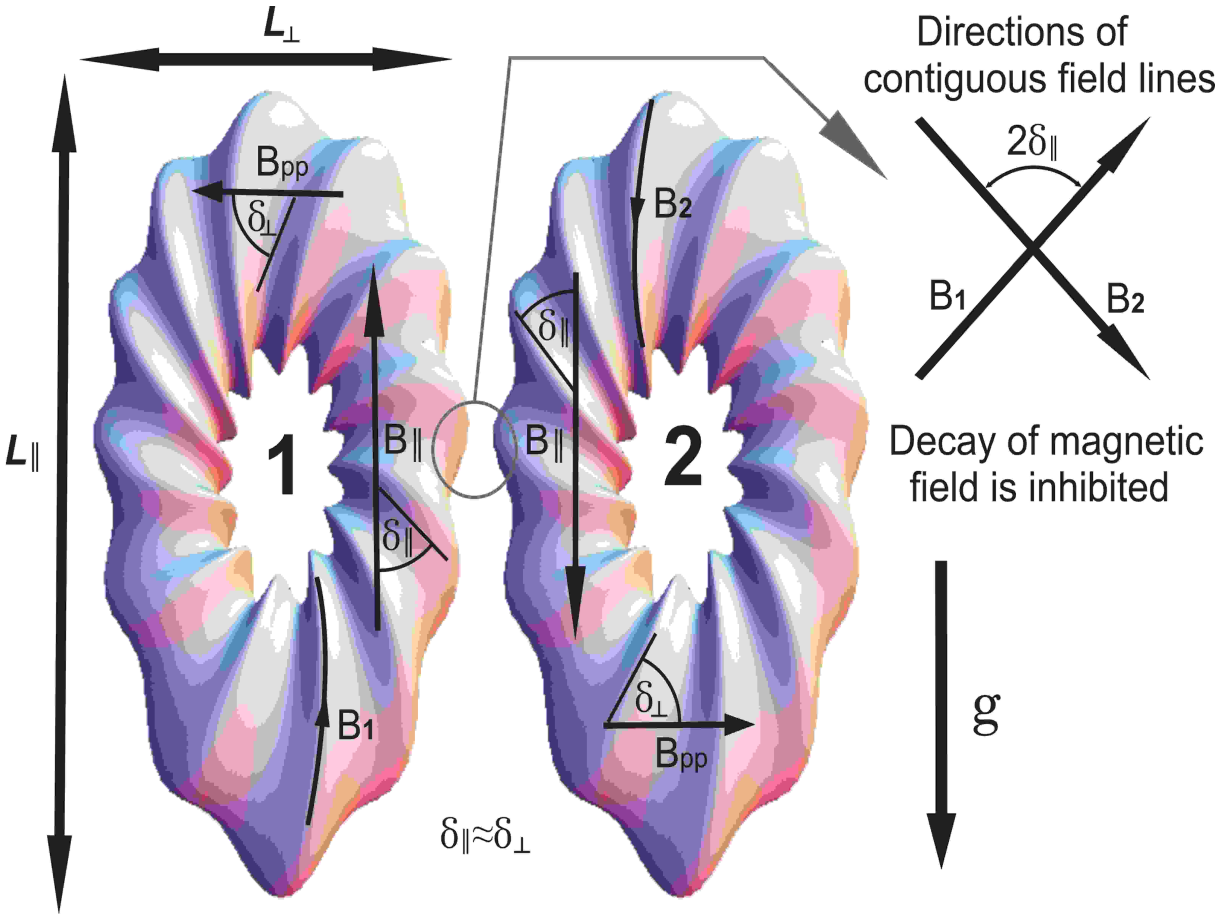

Fig. 1.— Two closed flux tubes with helicity of the same sign, dissipation of magnetic field is inhibited. Characteristic scales are: $L_\perp$ - perpendicular size of tubes, $L_{||}$ - radial size.

It is convenient to further transform the expression (B1) for magnetic helicity in flux tubes to find the best form of magnetic helicity conservation relation. Each flux tube (see Fig.1) has characteristic radial and perpendicular sizes $L_{||}$ and $L_{\perp}$. Its radial part has winded magnetic field with a winding angle $\delta_{||}$ between mean radial field $\vec{B}_{||}$ and the direction of magnetic field line. Perpendicular part of a flux tube has a winding angle $\delta_{\perp}$ between $\vec{B}_{pp}$ and the direction of field line. Flux tube occupies the volume

$$V_i = L_{||} \cdot L_{\perp}^2. \tag{B3}$$

Total number of tubes in the region S is

$$n = \frac{m}{\rho V_i} \tag{B4}$$

I take all internal radial sizes of flux tubes to scale as $L_{||}$ and internal perpendicular sizes as $L_{\perp}$. Hence, the number of windings $N_{||}$ on any radial segment of a tube and $N_{\perp}$ on any perpendicular segment are

$$N_{||} \propto \frac{L_{||}}{L_{\perp}} \tan\delta_{||} \quad \text{and} \quad N_{\perp} \propto \frac{L_{\perp}}{L_{||}} \tan\delta_{\perp} \tag{B5}$$

with approximately the same coefficient. Here I take already averaged (B2) over all the tubes $N_{||}$ and $N_{\perp}$. Magnetic flux Φ can be calculated from both mean radial $B_{||}$ and mean perpendicular B_{pp} magnetic fields

$$\Phi \propto B_{||} \cdot L_{\perp}^2 \quad \text{and} \quad \Phi \propto B_{pp} \cdot L_{||} L_{\perp}. \tag{B6}$$

Coefficients in both expressions are the same. I substitute magnetic flux from (B6) into expression for magnetic helicity (B1) considering that $B_{pp}^2 = B_{\theta}^2 + B_{\phi}^2 = 2B_{\perp}^2$. I obtain

$$H \propto n(N_{||}(B_{||}L_{\perp}^2)^2 + 2N_{\perp}(B_{\perp}L_{\perp}L_{||})^2). \tag{B7a}$$

Finally, I substitute numbers of windings $N_{||}$ and $N_{\perp}$ from (B5), total number of tubes from (B4) and volume of one flux tube from (B3) and arrive at

$$H \propto L_{\perp}(v_{Ar}^2 \tan\delta_{||} + 2v_{A\perp}^2 \tan\delta_{\perp}) \tag{B7b}$$

for constant mass m = const and definitions of Alfven velocities (24). Configuration with minimum energy for constant magnetic helicity (subject of future work) corresponds to

$$\delta_{||} = \delta_{\perp} = \delta. \tag{B8}$$

Applying (B8) to transformed expression for H (B7) I can write the equivalent form of magnetic helicity conservation

$$L_{\perp}(v_{Ar}^2 + 2v_{A\perp}^2) \tan\delta = \text{const}. \tag{B9}$$

C. Self-Similar solution

Let me describe the self-similar solution, when the differential system of equations (53) can be reduced to the algebraic system. I need to assume the right scalings of quantities with radius and make weak additional assumptions. I introduce the standard non-dimensional variables $T(x), \rho(x), L(x), aa(x), bb(x), pp(x), vel(x)$ to replace, respectively, $T(r), \rho(r), L(r)$, $u(r), v_{Ar}(r), v_{A\perp}(r), v(r)$ as follows:

$$T(r) = T_\infty T(x) \qquad v(r) = vel(x)\left(\frac{2RT(x)}{\mu}\right)^{1/2} \qquad L(r) = (r/x)L(x) \tag{C1}$$
$$u(r) = aa(x)\left(\frac{2RT(x)}{\mu}\right)^{1/2} \qquad v_{Ar}(r) = bb(x)\left(\frac{2RT(x)}{\mu}\right)^{1/2} \qquad v_{A\perp}(r) = pp(x)\left(\frac{2RT(x)}{\mu}\right)^{1/2}.$$

Radius is normalized to Bondi radius (55) as $r = r_B \cdot x$. The natural power-law radial dependencies of these (C1) quantities

$$\begin{aligned} T(x) &= T_{\rm SS}x^{-1} & vel(x) &= v_{\rm SS}x^{-1/2} & L(x) &= \gamma \\ aa(x) &= u_{\rm SS}x^{-1/2} & bb(x) &= v_{Ar\rm SS}x^{-1/2} & pp(x) &= v_{A\perp\rm SS}x^{-1/2} \end{aligned} \tag{C2}$$

make my system of equations (53) independent of x under the following restrictions:

- gravity is Newtonian,
- external turbulence driving is negligible,
- equation of state is non-relativistic.

These assumptions are valid in the intermediate region $10^3 r_{\rm g} \lesssim r \lesssim 0.1 r_B$. Gravity is Newtonian for $r \gg r_{\rm g}$. Turbulence driving is mainly internal for $r \lesssim 0.1 r_B$ (see subsections 4.1, 4.2 and Fig3b, Fig7b). Electrons become relativistic at around $10^3 r_{\rm g}$. The found range of r where all above assumptions hold is small. I can consider non-relativistic equation of state with $w = w_{gNR}$ (53c) everywhere. This makes standard self-similar solution possible from $0.1 r_B$ down to several Schwarzschild radii $r_{\rm g}$.

Dimensionless magnetic helicity ξ appears to be constant in self-similar regime. Relations (53h),(53g) and (47) lead to

$$\xi = \frac{3\sigma_\infty}{4T_{SS}(v^2_{ArSS} + 2v^2_{A\perp SS})}\xi_\infty. \tag{C3}$$

Continuity equation (53a) can be used to obtain the scaling of density $\rho \sim x^{-3/2}$. Heat balance equation (18) reduces to the equality of radial and total perpendicular magnetic field

$$v^2_{ASS} = 2v^2_{A\perp SS}. \tag{C4}$$

Euler equation (53b) gives the formula for self-similar temperature

$$T_{SS} = 5/(15 + 10u_{SS}^2 + 9v_{ArSS}^2 + 6v_{A\perp SS}^2 + 6v_{SS}^2). \tag{C5}$$

Turbulence evolution equations (23), (25), (27) are now treated without source terms. They give, correspondingly, three relations

$$\begin{aligned} 2u_{SS}v_{ArSS}c_{Bu11} - 2v_{ArSS}^2 c_{BB11}\exp(-\xi) + 4u_{SS}c_{Bu22}v_{A\perp SS} + 3v_{ArSS}v_{SS}\gamma = 0 \\ 2u_{SS}(v_{ArSS}c_{Bu22} + (c_{Bu11} + c_{Bu22})v_{A\perp SS}) - v_{A\perp SS}(2c_{BB11}\exp(-\xi)v_{A\perp SS} + 3v_{SS}\gamma) = 0 \\ -u_{SS}^2 c_{uu} + c_{uB11}\exp(-\xi)(v_{ArSS}^2 + 2v_{A\perp SS}^2) = 0, \end{aligned} \tag{C6}$$

where definitions of Alfven and turbulent velocities (24) are used.

Let me first set magnetic helicity to zero $\xi = 0$ and consider four equations (C4) and (C6) on four velocities v_{SS}, u_{SS}, v_{ArSS}, $v_{A\perp SS}$. The only solution of this system has all the velocities identical zeroes. No self-similar solution is possible for zero magnetic helicity ξ.

However, the non-linear algebraic system of equations on ξ and velocities (C3), (C4), (C6) possess a self-similar solution. When I have the full system (53), I need the additional condition to determine the accretion rate and solve for radial dependencies of quantities. This conditions is either condition for maximum accretion rate (66) or condition for effective angular momentum transport (63). I can transform both into self-similar form. Maximum $\dot{M}$ condition (66) reads

$$5 + 10u_{SS}^2 + 12v_{A\perp SS} = 6v_{SS}^2. \tag{C7a}$$

Momentum transport condition (63) is

$$\frac{\sqrt{5/3}\cdot v_{SS}}{4v_{ArSS}\cdot v_{A\perp SS}\sqrt{T_{SS}}} \le 1 \tag{C7b}$$

regardless of circularization radius $r_{\rm cir}$.

Let me first find the self-similar solution in case of large angular momentum. I solve equality in (C7b) and 5 equations (C3), (C4), (C6) for 6 quantities ξ, u_{SS}, v_{ArSS}, $v_{A\perp SS}$, $\gamma\cdot v_{SS}$ and the product of $\sigma_\infty\xi_\infty$. I normalize the results to free-fall velocity (69) to be able to directly compare with the numbers on Fig7b.

$$\frac{c_s(r)}{v_{ff}(r)} = 0.58, \quad \frac{u(r)}{\sqrt{3}v_{ff}(r)} = 0.0094, \quad \frac{v_{Ar}(r)}{v_{ff}(r)} = 0.041, \tag{C8}$$

$$\frac{v_{A\perp}(r)}{v_{ff}(r)} = 0.029, \quad \frac{v(r)}{v_{ff}(r)} = 0.0033, \quad \sigma_\infty\xi_\infty = 0.00718 \tag{C9}$$

for $r > r_{\rm g}$. Fig7b shows profile of velocities for outer conditions $\sigma_\infty = 1$, $\xi_\infty = 0.025$, $\gamma = 1$. The actual velocities on the inner boundary at $r = 3\cdot 10^{-4} r_B = 90 r_{\rm g}$ are

$$\begin{aligned} &\frac{c_s(r)}{v_{ff}(r)} = 0.58, \quad \frac{u(r)}{\sqrt{3}v_{ff}(r)} = 0.0033, \quad \frac{v_{Ar}(r)}{v_{ff}(r)} = 0.076, \\ &\frac{v_{A\perp}(r)}{v_{ff}(r)} = 0.024, \quad \frac{v(r)}{v_{ff}(r)} = 0.0051. \end{aligned} \tag{C10}$$

The value $\sigma_\infty\xi_\infty = 0.025$ is only about 3 times larger than in self-similar solution (C8), magnetic field is stronger. Therefore, higher values of all characteristic velocities are expected in the actual solution (C10). I obtain inflow velocity v and radial Alfven speed v_{Ar} correspondingly 1.5 and 1.8 times higher for (C10). Sonic speeds are the same in self-similar (C8) and actual (C10) solutions, because almost all gravitational energy goes into thermal energy in both solutions. However, perpendicular Alfven velocity $v_{A\perp}$ and turbulent velocity u do not qualitatively agree with self-similar solution. They are correspondingly 1.2 and 2.8 times lower in the actual solution (C10). The naive estimate for accretion rate is

$$4\pi\rho_\infty v(r_B) r_B^2 \approx 0.05\dot{M}_B. \tag{C11}$$

This appears to be 8 times larger than the actual accretion rate $0.0061\dot{M}_B$. Velocity near Bondi radius (55) is much smaller than self-similar value that leads to an overestimate of $\dot{M}$. Thus, self-similar solution can give an order of magnitude estimates for all characteristic velocities of the flow and even for accretion rate $\dot{M}$. However, self-similar solution has only 2 parameters instead of 3, because $\sigma_\infty\xi_\infty$ is treated as one constant. Therefore, solution of the full system (53) is required to probe the entire parameter space and to achieve more precise results.

Self-similar solution in case of maximum rate flow with condition (C7a) does not exist. The formal solution of (C7a) with (C3), (C4), (C6) leads to negative product $\sigma_\infty\xi_\infty$. The absence of self-similar solution in this case is reasonable, since the actual solution does not exhibit self-similar scalings Fig3b.

D. Convection

Let me elaborate the stability criterion against convection in my model. As I noted in the main text 5.4, small scale perturbations of quantities are smeared out by diffusion. Thus high-frequency analysis (Scharlemann 1983) is not appropriate to determine the convective stability. Timescale of diffusion $\tau_{\rm diff}$ is

$$\tau_{\rm diff} \sim \frac{l}{u}, \tag{D1}$$

where l is the scale of perturbation. As l decreases, diffusion time also decreases and becomes smaller than perturbation growth timescale $\tau_{\rm grow}$. If $\tau_{\rm diff} < \tau_{\rm grow}$, convection is ineffective that is likely to happen at small scales l. Thus I need to consider the motion of the large blobs of the size $l \sim L$.

I consider a blob of plasma displaced at some small Δr from its equilibrium position Fig.2. The density of outer medium changes by $\Delta\rho_{\rm fluid}$ between two positions of the blob. The density of the blob itself changes by $\Delta\rho_{\rm blob}$. The goal is to calculate the difference in density differences $\Delta\rho_{\rm fluid} - \Delta\rho_{\rm blob} > 0$ between the outer medium and the blob. Positive difference $\Delta\rho_{\rm fluid} - \Delta\rho_{\rm blob} > 0$ for positive $\Delta r > 0$ implies convective instability. Rising blob of gas is rarified compared to the fluid and buoyant. The results for $\Delta\rho$ may be affected by external driving that is somewhat artificial in my model. Thus I need to calculate $\Delta\rho$ in the inner accretion region where external driving is not important. Motion of the blob is adiabatic and

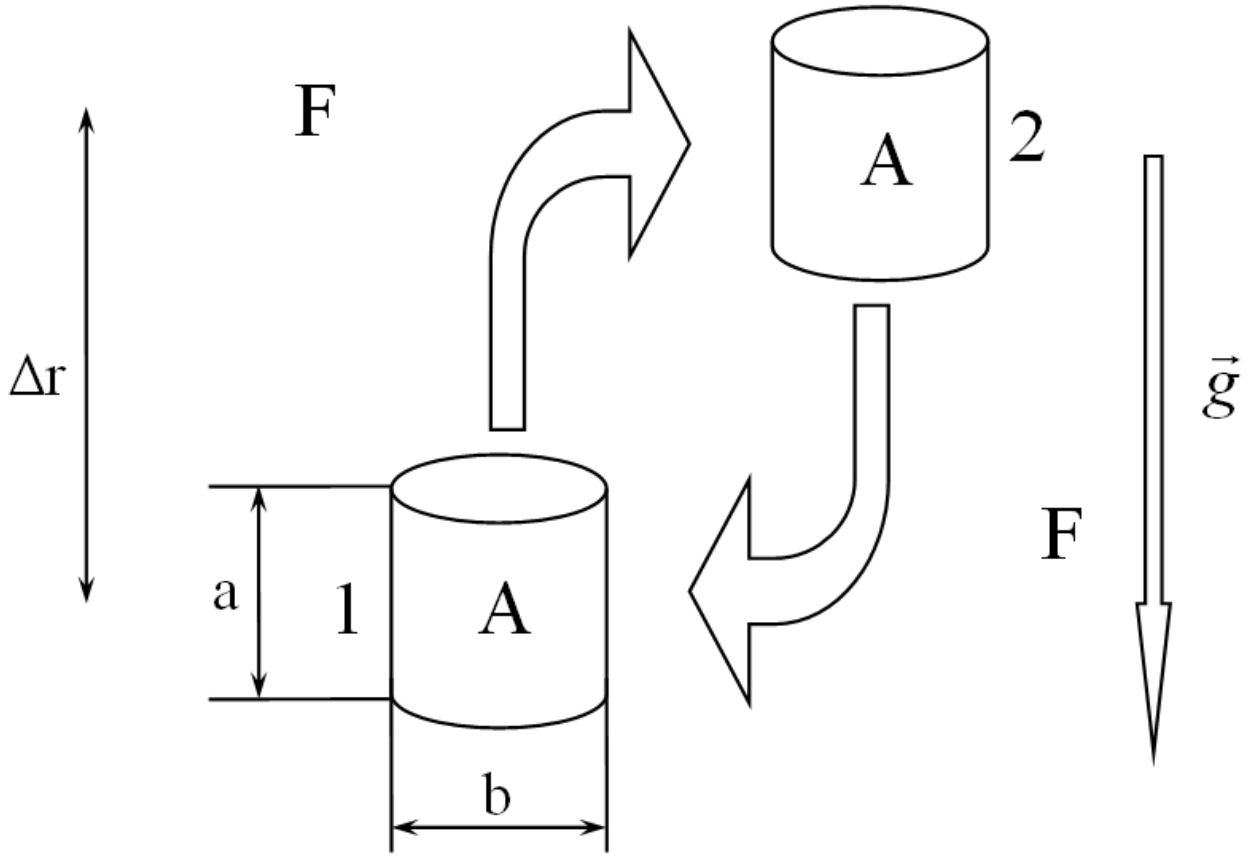

Fig. 2.— Scheme of convection.

governed by the same adiabatic dynamical equations (53b) and (53c), as the rest of the fluid. I neglect energy, associated with gas regular velocity v. Term v^2 cannot be neglected only in the region, where v approaches sound speed c_s. However, convection ceases if $v \sim c_s$ (Narayan et. al. 2002). I denote by index A physical quantities in the blob and by index F quantities in the rest of the fluid.

Euler equation (53b) results in the following changes in pressure of the blob

$$\frac{R}{\mu}\Delta_A(\rho T) + \frac{1}{3}\Delta_A(\rho u^2) + \frac{1}{r^2}\Delta_A(r^2\rho v_{A\perp}^2) - \frac{1}{2r^4}\Delta_A(r^4\rho v_A^2) = 0 \qquad \text{(D2a)}$$

and of the fluid

$$\frac{R}{\mu}\Delta_F(\rho T) + \frac{1}{3}\Delta_F(\rho u^2) + \frac{1}{r^2}\Delta_F(r^2\rho v_{A\perp}^2) - \frac{1}{2r^4}\Delta_F(r^4\rho v_A^2) = 0. \qquad \text{(D2b)}$$

In both equations I take differences between the displaced by Δr position and initial position. I introduce the difference operator

$$\Delta() = \Delta_F() - \Delta_A() \qquad \text{(D3)}$$

and calculate the differences of all the quantities between the fluid and the blob. Subtracting

(D2)b from (D2)a, I find the radial pressure balance in the first order in Δr

$$\frac{R}{\mu}\Delta(\rho T) + \frac{1}{3}\Delta(\rho u^2) + \Delta(\rho v_{A\perp}^2) - \frac{1}{2}\Delta(\rho v_A^2) = 0. \tag{D4}$$

Blob of plasma should be in equilibrium in all three directions, not only in radial direction. I need the pressure balance in perpendicular direction. I use the same technique to deduce it, as I used to derive the radial force equation (14) from general momentum equation (3). Component θ of magnetic force in (2) and (3) reads $F_\theta = [\vec{B} \times [\vec{\nabla} \times \vec{B}]]_\theta/(4\pi\rho)$. I subtract $B_\theta(\vec{\nabla} \cdot \vec{B})/(4\pi\rho)$ from it and average over ϕ direction. I obtain

$$F_\theta = \frac{(B_r^2)'_\theta}{8\pi\rho r} \tag{D5}$$

for $B_\theta^2 = B_\phi^2$ and $B_r B_\theta = 0$ on average over ϕ. All other terms in (3) are trivial. The final form of force balance in θ direction is

$$\frac{\partial}{\partial\theta}\left(\frac{R}{\mu}\rho T + \frac{1}{3}\rho u^2 + \frac{1}{2}\rho v_A^2\right) = 0. \tag{D6}$$

Perpendicular force balance (D6) has the same form in any perpendicular direction owing to the symmetry of the problem.

I apply operator Δ (D3) to the integral form of perpendicular pressure balance and get

$$\frac{R}{\mu}\Delta(\rho T) + \frac{1}{3}\Delta(\rho u^2) + \frac{1}{2}\Delta(\rho v_A^2) = 0. \tag{D7}$$

Heat balance equation (18) gives the third relation

$$\frac{R}{\mu}\left(\frac{3}{2}\Delta T - \frac{\Delta\rho}{\rho}T\right) + \left(u\Delta u - \frac{u^2}{3}\frac{\Delta\rho}{\rho}\right) + \rho\Delta\left(\frac{v_{A\perp}^2}{\rho}\right) + \frac{1}{2\rho}\Delta(\rho v_A^2) = 0. \tag{D8}$$

Stretching and contraction of blob are non-uniform. Perpendicular b and parallel a sizes (see Fig2) deform in different ways. Continuity equation for the fluid (10) can be written as

$$\frac{\Delta_F\rho}{\rho} + \frac{\Delta_F v}{v} + 2\frac{\Delta r}{r} = 0 \tag{D9a}$$

I consider the parcel with constant mass $m = \rho V$. Therefore

$$\frac{\Delta_A\rho}{\rho} + \frac{\Delta a}{a} + 2\frac{\Delta b}{b} = 0 \tag{D9b}$$

is the continuity relation for the parcel. Finally I subtract (D9a) from (D9b) and obtain

$$\frac{\Delta\rho}{\rho} + \frac{\Delta v}{v} + 2\frac{\Delta r}{r} - \frac{\Delta a}{a} - 2\frac{\Delta b}{b} = 0 \tag{D10}$$

according to (D3) for the change of density. Inflow velocity v is clearly associated with the fluid, but I omit subscript F at v. I also omit subscript A at dimensions of the blob.

Now I need to quantify the variation of the turbulent magnetic field and the random velocity. I assume that the blob moves at a speed $V(r)$ much higher than the inflow velocity $V(r) \gg v(r)$, therefore magnetic field does not dissipate in the parcel. Differences of turbulence evolution equations (53d), (53e) and (53f) are

$$2u\Delta u - \frac{2}{3}u^2\frac{\Delta\rho}{\rho} = \frac{\Delta r}{vL}(c_{uu}u^3 - c_{uB11}(v_A^2 + 2v_{A\perp}^2)u\exp(-\xi)) \tag{D11a}$$

$$\Delta(\rho v_A^2) + 4\rho v_A^2\left(\frac{\Delta r}{r} - \frac{\Delta b}{b}\right) = \frac{\rho\Delta r}{vL}(c_{BB11}v_A^3\exp(-\xi) - (c_{Bu11}v_{Ar}^2 + 2c_{Bu22}v_{Ar}v_{A\perp})u) \tag{D11b}$$

$$\Delta(\rho v_{A\perp}^2)+2\rho v_{A\perp}^2\left(\frac{\Delta r}{r} + \frac{\Delta v}{v} - \frac{\Delta a}{a} - \frac{\Delta b}{b}\right) = \frac{\rho\Delta r}{vL}(c_{BB11}v_{A\perp}^3\exp(-\xi)-((c_{Bu11}+c_{Bu22})v_{A\perp}^2-c_{Bu22}v_{Ar}v_{A\perp})u) \tag{D11c}$$

Magnetic helicity variation does not directly influence the dynamics of the blob. Solving the system of 7 equations (D4), (D7), (D8), (D10), (D11)abc on 7 quantities $\Delta T, \Delta\rho, \Delta v_A, \Delta v_{A\perp}$, $\Delta u, \Delta a, \Delta b$, I obtain

$$\frac{1}{\rho}\frac{\Delta\rho_{\rm correct}}{\Delta r} \approx \frac{v_{Ar}(2.02\exp(-\xi)v_{Ar}v_{A\perp}(v_{Ar}+2v_{A\perp}) - u(0.39(v_{Ar}^2v_{A\perp}+v_{A\perp}^3) + v_{Ar}(1.21v_{A\perp}^2 - 0.63u^2)))}{c_s^2Lv(v_{Ar}^2+v_{A\perp}^2)}. \tag{D12}$$

The actual expression is much longer. I take only the largest terms in the numerator and the denominator.

Let me compare this result (D12) with the naive estimate, when magnetic field dissipation increases gas internal energy only (Bisnovatyi-Kogan & Ruzmaikin 1974) and gas pressure balance is used instead of (D4), (D7).

Pressure balance is written as

$$\Delta(\rho T) = 0 \tag{D13}$$

Naive heat balance (17) in the unit mass chunk of matter is

$$\frac{R}{\rho\mu}\left(\frac{3}{2}\rho\Delta T - T\Delta\rho\right) \approx \frac{\Delta r}{Lv}(0.41v_{Ar}^2u+1.16v_{Ar}uv_{A\perp}+1.4uv_{A\perp}^2-3.03(v_{Ar}^3+2v_{A\perp}^3)\exp(-\xi)-1.14u^3) \tag{D14}$$

Eliminating ΔT from (D13) and (D14), I find

$$\frac{1}{\rho}\frac{\Delta\rho_{\rm naive}}{\Delta r} \approx \frac{0.61(v_{Ar}^3+2v_{A\perp}^3)\exp(-\xi) + 0.23u^3 - 0.82v_{Ar}^2u - 0.23v_{Ar}uv_{A\perp} - 0.28uv_{A\perp}^2}{c_s^2Lv} \tag{D15}$$

I evaluate the convective derivatives of density (D12) and (D15) in the inner region of the reference solution with angular momentum transport 4.2. Parameters of the reference model are $\xi_\infty = 0.025$, $\sigma_\infty = 1$, $\gamma = 1$, non-relativistic EOS. Correspondent velocities are shown on Fig.7b. I take velocities and magnetic helicity on the inner boundary of integration $r = 3\cdot10^{-4}r_B \approx 90r_{\rm g}$. Change of density appears to be negative $\Delta\rho < 0$ for $\Delta r > 0$ in the result of full calculation (D12). Naive calculation shows positive $\Delta\rho > 0$ for $\Delta r > 0$.

$$\frac{\Delta\rho_{\rm correct}}{\Delta\rho_{\rm naive}} \approx -0.2. \tag{D16}$$

Naive calculation suggests that the flow is convectively unstable, whereas the full calculation under reasonable assumptions indicates a convectively stable flow.

The calculated result (D16) is applicable only to the inner regions of solution with angular momentum transport 4.2. Excluded external driving is important in the outer regions. In turn, solution with maximum accretion rate has large inflow velocity v that approaches gas sound speed c_s. Velocity of convective blobs v_b is supposed to be much larger than inflow velocity $v_b \gg v$. However, blobs cannot attain energy compared to gas thermal energy. It means that blob speed is smaller than the speed of sound $v_b < c_s$. The above two inequalities are inconsistent with $v \sim c_s$. Thus the used approach breaks. It is easy to show (Narayan et. al. 2002) that convection is strongly suppressed for $v \sim c_s$. As a bottom line, either flow appears to be convectively stable on average or convection is suppressed in all calculated solutions. This result is consistent with numerical simulations of MHD disks (Hawley & Balbus 2002).

However, some numerical simulations find evidence of convection (Igumenshchev 2006). This convection may be physical. My model averages heat from all dissipation events over the fluid. Local reconnection events can lead to burst-type local heating that lead to buoyancy of blobs. Also, magnetic buoyancy and diffusion play important role in transfer processes (Igumenshchev 2006). The correct inclusion of convection, magnetic buoyancy and diffusion is the subject of future studies.

REFERENCES

Abramowicz, M.A. et al., "On the Radial Structure of Radiatively Inefficient Accretion Flows with Convection", 2002, ApJ, v. 565, p. 1101

Aschwanden M. J., "Physics of the Solar Corona: An Introduction with Problems and Solutions", 2005, Springer

Baganoff, F. K. et al., "Chandra X-Ray Spectroscopic Imaging of Sagittarius A* and the Central Parsec of the Galaxy", 2003, ApJ, v. 591, p. 891

Beskin, G. M., Karpov S. V., "Low-rate accretion onto isolated stellar-mass black holes", 2005, A&A v. 440, p. 223

Beskin, V. S., Pidoprygora, Yu. N., "Hydrodynamic accretion onto black holes", 1995, JETP, v. 80, p. 575

Biskamp, D., "Magnetic reconnection in plasmas", 2000, Cambridge University Press

Biskamp, D., "Magnetohydrodynamic turbulence", 2003, Cambridge University Press

Bisnovatyi-Kogan, G. S., Ruzmaikin, A. A., "The Accretion of Matter by a Collapsing Star in the Presence of a Magnetic Field", 1974, Ap&SS, v. 28, p. 45

Bisnovatyi-Kogan, G. S., Lovelace, R. V. E., "Magnetic Field Limitations on Advection-dominated Flows", 2000, ApJ, v. 529, p. 978

Blandford, R. D., Begelman, M. C., "On the fate of gas accreting at a low rate on to a black hole", 1999, MNRAS, v. 303, p. 1

Boldyrev, S., Yusef-Zadeh, F., "Turbulent Origin of the Galactic Center Magnetic Field: Non-thermal Radio Filaments", 2006, ApJ, v. 637, p. 101

Boldyrev S., "Spectrum of Magnetohydrodynamic Turbulence", 2006, Phys. Rev. Lett. v. 96, p. 115002

Bondi, H., "On spherically symmetrical accretion.", 1952, MNRAS, v. 112, p. 195

Bower et al., "Variable Linear Polarization from Sagittarius A*: Evidence of a Hot Turbulent Accretion Flow", 2005, ApJ, v. 618, p. 29

Braithwaite, J., Spruit H. "A fossil origin for the magnetic field in A stars and white dwarfs", 2004, Nature, v. 431, p. 819

Chandrasekhar, S., "Introduction to the Study of Stellar Structure", 1939, Dover Publications

Coker, R.F., Melia, F., "The Role of Magnetic Field Dissipation in the Black Hole Candidate Sagittarius A*", 2000, ApJ, v. 534, p. 723

Cuadra, J. et al., "Accretion of cool stellar winds on to Sgr A*: another puzzle of the Galactic Centre?", 2005, MNRAS, v. 360, p. 55

Cuadra, J. et al., "Galactic Centre stellar winds and Sgr A* accretion", 2006, MNRAS, v. 366, p. 358

Eckart A., "The flare activity of Sagittarius A*. New coordinated mm to X-ray observations", 2006, A&A, v. 450, p. 535

Falcke, H., Markoff, S., "The jet model for Sgr A*: Radio and X-ray spectrum", 2000, A&A, v. 362, p. 113

Gammie, C. F., Popham, R., "Advection-dominated Accretion Flows in the Kerr Metric. I. Basic Equations", 1998, ApJ, v. 498, p. 313

Ghez, A. M. et al., "Full Three Dimensional Orbits For Multiple Stars on Close Approaches to the Central Supermassive Black Hole", 2003, ANS, v. 324, p. 527

Goldreich, P., Sridhar, S., "Towards a theory of interstellar turbulence. II. Strong Afvenic turbulence", 1995, ApJ, v. 438, p. 763

Hawley, J. F., Balbus, S. A., "The Dynamical Structure of Nonradiative Black Hole Accretion Flows", 2002, ApJ, v. 573, p. 738

Igumenshchev, I. V., Narayan, R., "Three-dimensional Magnetohydrodynamic Simulations of Spherical Accretion", 2002, ApJ, v. 566, p. 137

Igumenshchev, I.V., Narayan, R., Abramowicz, M.A., "Three-dimensional Magnetohydrodynamic Simulations of Radiatively Inefficient Accretion Flows", 2003, ApJ, v. 592, p. 1042

Igumenshchev, I., "Three-dimensional Simulations of Spherical Accretion Flows with Small-Scale Magnetic Fields", 2006, ApJ, v. 649, p. 361

Ipser, J. R., Price, R. H., "Synchrotron radiation from spherically accreting black holes", 1982, ApJ, v. 255, p. 654

Kida, S., Yanase, S., Mizushima, J., "Statistical properties of MHD turbulence and turbulent dynamo", 1991, Fluid Mechanics, v. 3, p. 457

Kowalenko, V., Melia, F., "Towards incorporating a turbulent magnetic field in an accreting black hole model", 1999, MNRAS, v. 310, p. 1053

Ladeinde F., Gaitonde D. V., "Magnetic Reynolds number effects in compressible magnetohydrodynamic turbulence", 2004, Physics of Fluids, v. 16, p. 2097

Landau, L. D., Lifshitz, E. M., "Classical theory of fields", 1971, Oxford: Pergamon Press

Landau, L. D., Lifshitz, E. M., "Fluid mechanics", 1987, Oxford: Pergamon Press

Landau L. D., Lifshitz E. M., Pitaevskii L. P., "Electrodynamics of Continuous Media", 1984, Oxford: Pergamon Press

Lazarian, A., Vishniac, E. T., "Reconnection in a Weakly Stochastic Field", 1999, ApJ, v. 517, p. 700

Lazarian, A.; Vishniac, E., "Fast Reconnection of Magnetic Fields in Turbulent Fluids", 2000, RMxAC, v. 9, p. 55

Lazarian, A., "Intermittency of Magnetohydrodynamic Turbulence:. an Astrophysical Perspective", 2006, IJMPD, v. 15, p. 1099

Marrone D.P. et.al.; "An Unambiguous Detection of Faraday Rotation in Sagittarius A*", 2007, ApJ, v. 654, p. 57

McKinney J. C., "General relativistic magnetohydrodynamic simulations of the jet formation and large-scale propagation from black hole accretion systems", 2006, MNRAS, v. 368, p. 1561

Moscibrodzka, M., Das, T. K., Czerny, B., "The pattern of accretion flow on to Sgr A*", 2006, MNRAS, v. 370, p. 219

Narayan, R., Yi, I., "Advection-dominated Accretion: Underfed Black Holes and Neutron Stars", 1995, ApJ, v. 452, p. 710

Narayan, R. et al., "Advection-dominated accretion model of Sagittarius A*: evidence for a black hole at the Galactic center", 1998, ApJ, v. 492, p. 554

Narayan, R., Igumenshchev, I. V., Abramowicz, M. A., "Self-similar Accretion Flows with Convection", 2000, ApJ, v. 539, p. 798

Narayan, R. et al., "The Magnetohydrodynamics of Convection-dominated Accretion Flows", 2002, ApJ, v. 577, p. 295

Noglik, J. B., Walsh, R. W., Ireland, J., "Indirect calculation of the magnetic reconnection rate from flare loops", 2005, A&A, v. 441, p. 353

Paczhynski, B., Wiita, P.J., 1980, A&A, v. 88, p. 23

Quataert, E., Gruzinov, A., "Turbulence and Particle Heating in Advection-dominated Accretion Flows", 1999, ApJ, v. 520, p. 248

Quataert, E., Gruzinov, A., "Convection-dominated Accretion Flows", 2000, ApJ, v. 539, p. 809

Quataert, E., Narayan, R., "The Cooling Flow to Accretion Flow Transition", 2000, ApJ, v. 528, p. 236

Quataert, E., "A Dynamical Model for Hot Gas in the Galactic Center", 2004, ApJ, v. 613, p. 322

Scharlemann, E.T., "The dynamics of dissipatively heated spherical accretion", 1983, ApJ, v. 272, p. 279

Schekochihin, A. A., "Simulations of the Small-Scale Turbulent Dynamo", 2004, ApJ, p. 612, v. 276

Schwartzman, V.F., 1971, Soviet Astronomer, v.15, p.377

Shakura, N. I., Syunyaev, R. A., "Black holes in binary systems. Observational appearance.", 1973, A&A, v. 24, p. 337

Sharma P. et al., "Electron Heating in Hot Accretion Flows", astro-ph/0703572

Shapiro S. L., Teukolsky S. A., "Black Holes, White Dwarfs and Neutron Stars", 1983, Wiley-Interscience

Sreenivasan, K. R., "On the universality of the Kolmogorov constant", 1995, Physics of Fluids, v. 7, p. 2778

Sutherland, R. S., Dopita, M. A., "Cooling functions for low-density astrophysical plasmas", 1993, ApJS, v. 88, p. 253

Tennekes H., Lumley J. L., "A First Course in Turbulence", 1972, The MIT Press

Vishniac, E.T., Cho J., "Magnetic Helicity Conservation and Astrophysical Dynamos", ApJ, 2001, v. 550, p. 752

Yuan, F., "Luminous hot accretion discs", 2001, MNRAS, v. 324, p. 119

Yuan, F., Markoff, S., Falcke, H., "A Jet-ADAF Model for Sgr A*", 2003, ANS, v. 324, v. 453

Yuan, F., Markoff, S., Falcke, H., "A Jet-ADAF model for Sgr A*", 2002, A&A, v. 383, p. 854

Yuan, F., Quataert, E., Narayan, R., "Nonthermal Electrons in Radiatively Inefficient Accretion Flow Models of Sagittarius A*", 2003, ApJ, v. 598, p. 301

Yuan, F. et al., "Hot One-Temperature Accretion Flows Revisited", 2006, ApJ, v. 636, p. 46

Zhi-Qiang Shen, "High-resolution Millimeter-VLBI Imaging of Sgr A*", 2006, astro-ph/0611613

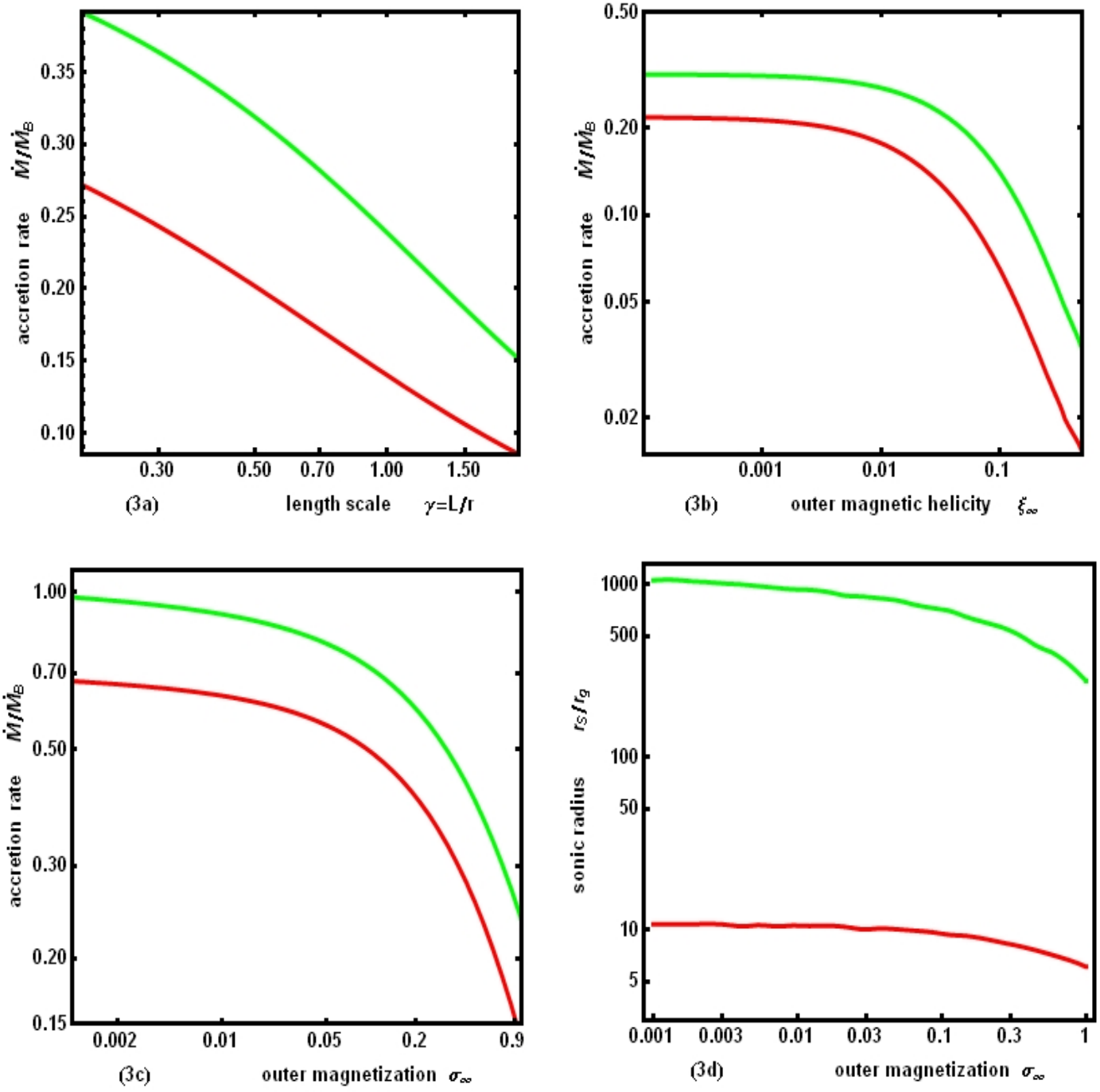

Fig. 3.— **Maximum accretion rate solution.** Dependence of the accretion rate in units of Bondi rate on dimensionless parameters: characteristic length scale γ (Fig. 3a), outer magnetic helicity ξ_∞ (Fig. 3b), outer matter magnetization σ_∞ (Fig. 3c). Dependence (Fig. 3d) of sonic radius on outer magnetization σ_∞. I take the reference model to have the following values of parameters: $\gamma = 1$, $\sigma_\infty = 1$, $\xi_\infty = 0.025$. One parameter is varied to make one plot. Non-relativistic equation of state (red) verses 1-T equation of state (green).

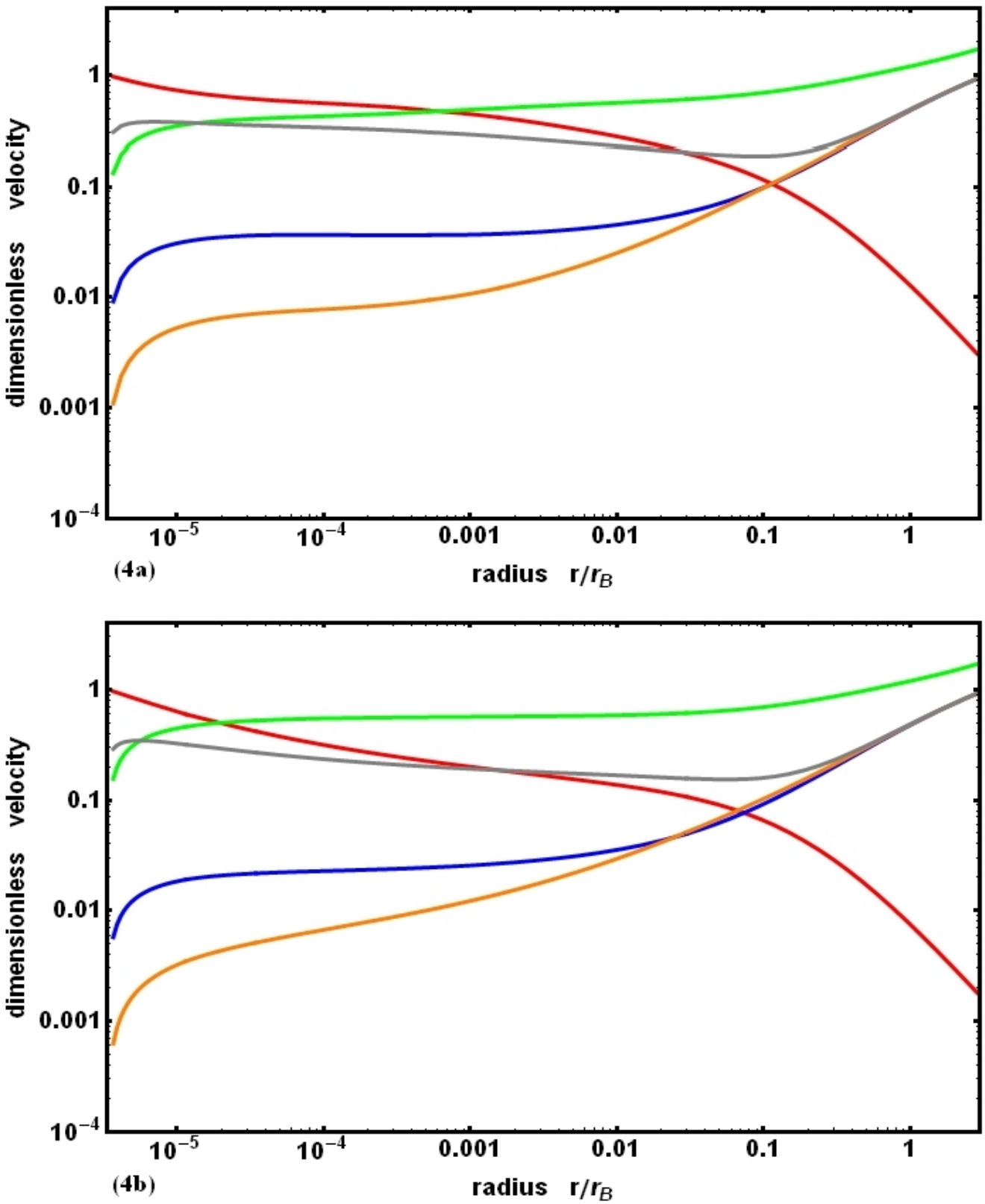

Fig. 4.— Flow velocities, normalized to free-fall speed verses radius for **maximum rate solution**: sound speed (green), inflow velocity (red), radial Alfven velocity (gray), 1-D perpendicular Alfven velocity (orange), turbulent velocity (blue). Parameters $\sigma_\infty = 1$, $\gamma = 1$, $\xi_\infty = 0.025$. Relativistic 1-T equation of state is on Fig4a, non-relativistic 1-T EOS is on Fig4b.

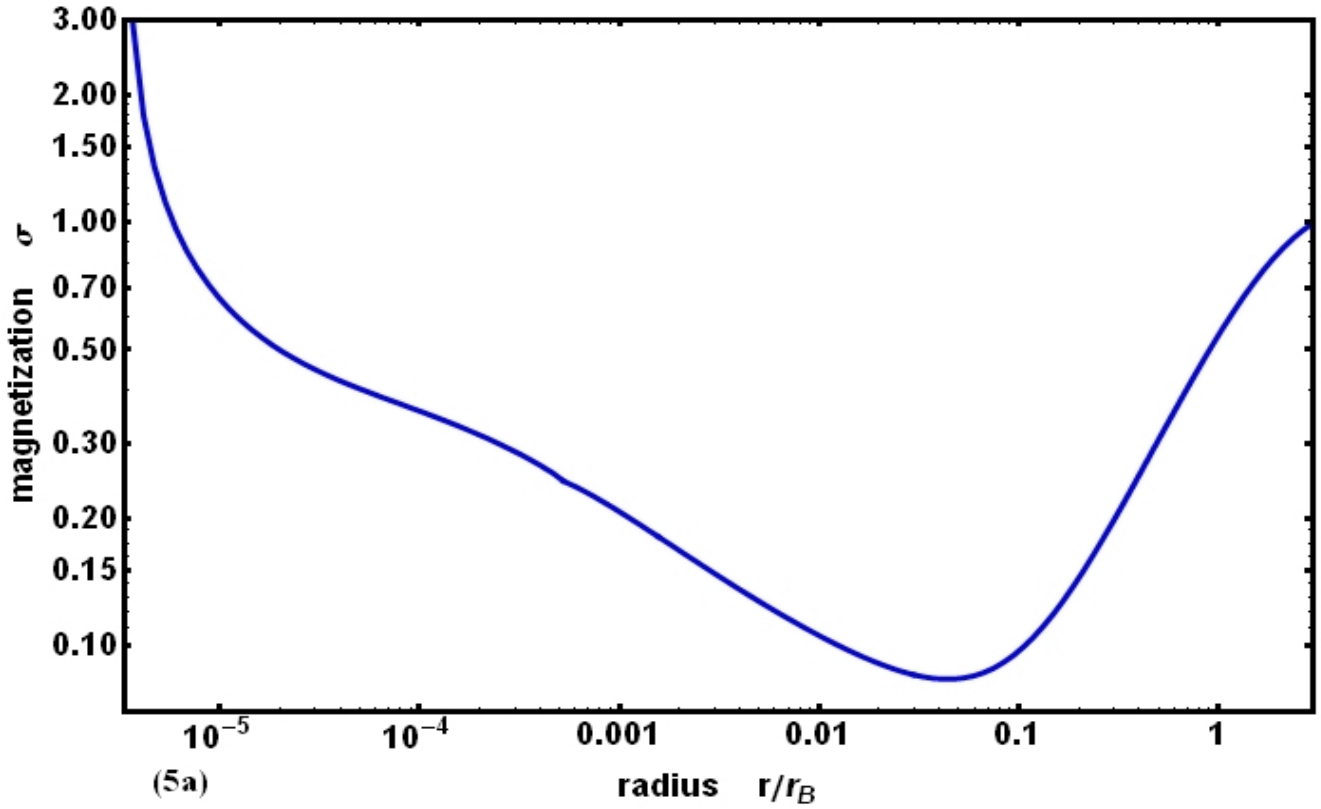

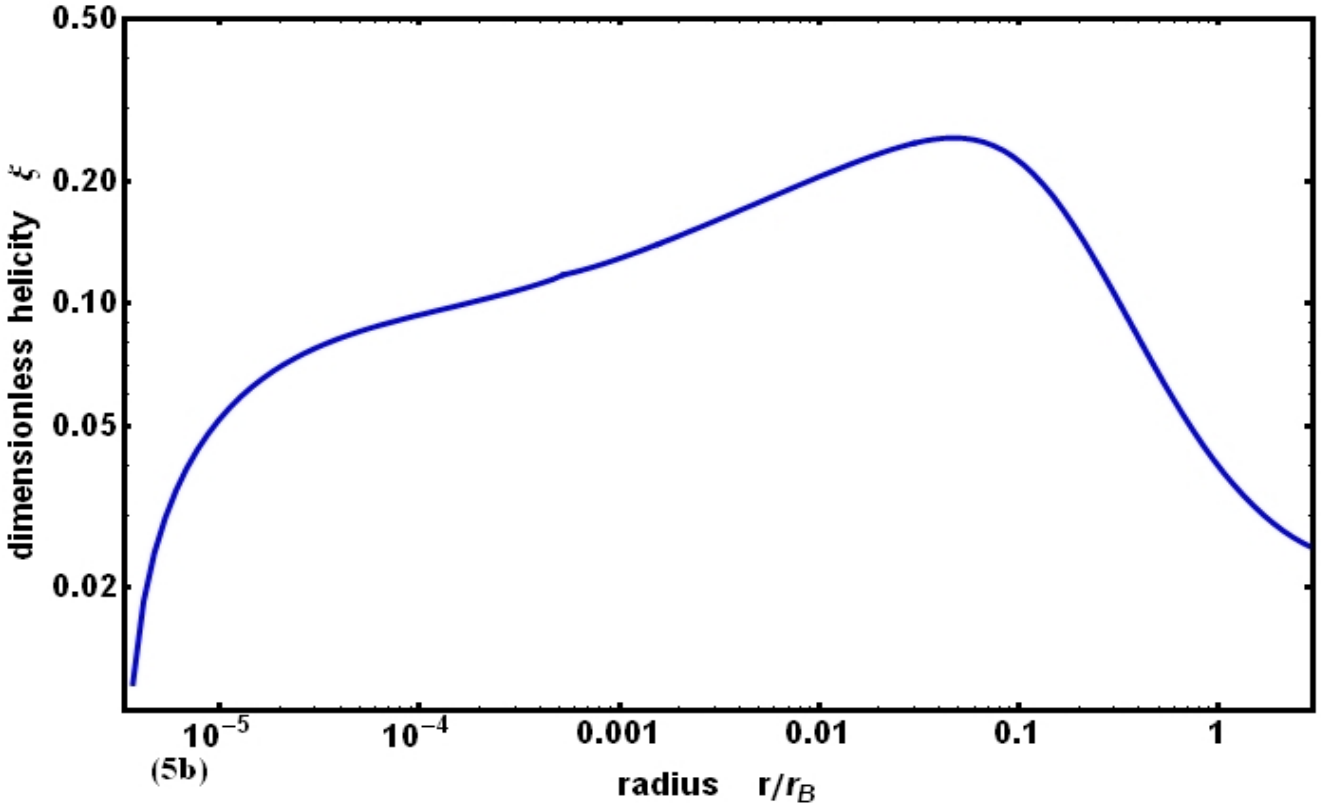

Fig. 5.— Magnetization σ verses dimensionless distance from the compact object r/r_B is on Fig5a. Dimensionless magnetic helicity ξ verses dimensionless distance from the compact object r/r_B is on Fig5b. Both are for the **maximum rate solution** with relativistic equation of state.

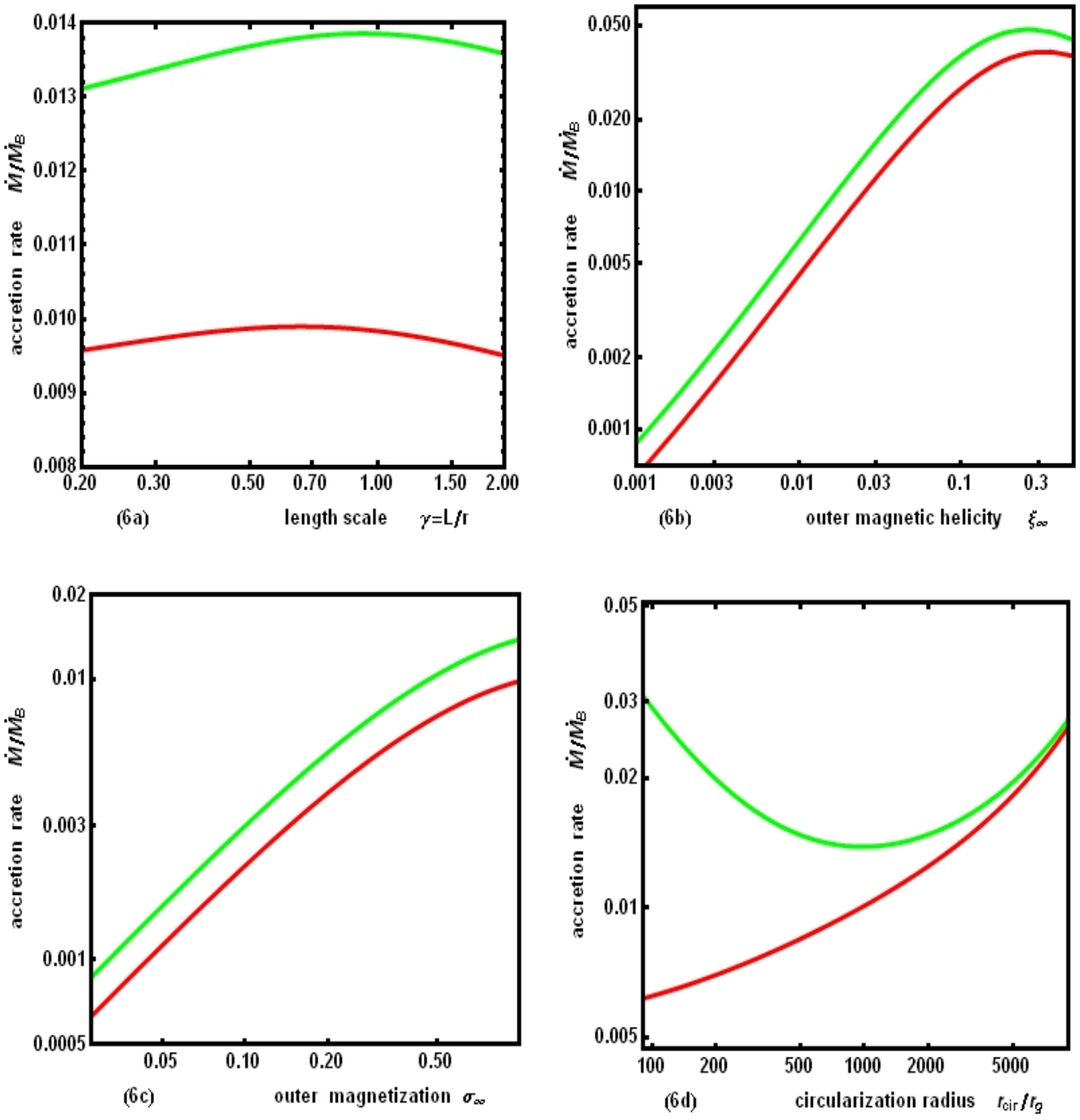

Fig. 6.— **Solution with angular momentum transport.** Dependence of the accretion rate in units of Bondi rate on dimensionless parameters: characteristic length scale γ (Fig. 6a), outer magnetic helicity ξ_∞ (Fig. 6b), outer magnetization σ_∞ (Fig. 6c) and circularization radius $r_{\rm cir}$ in units of $r_{\rm g}$ (Fig. 6d). I take the reference model to have the following parameters: $\gamma = 1$, $\sigma_\infty = 1$, $r_{\rm cir} = 10^3 r_{\rm g}$, $\xi_\infty = 0.025$. Non-relativistic 1-T equation of state (red) verses relativistic 1-T equation of state (green).

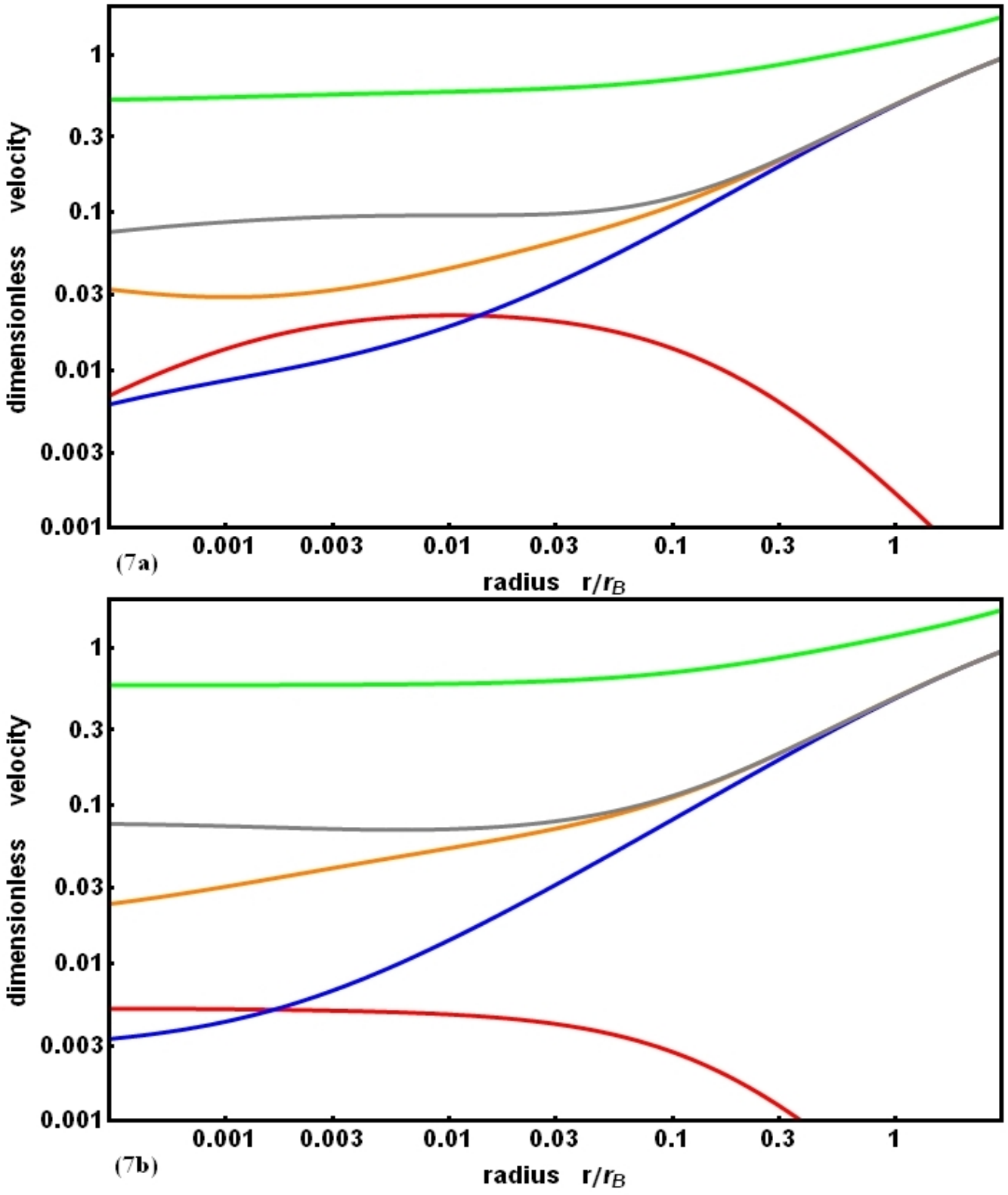

Fig. 7.— Flow velocities, normalized to free-fall speed verses radius for **solution with angular momentum transport**: sound speed (green), inflow velocity (red), radial Alfven velocity (gray), 1-D perpendicular Alfven velocity (orange), turbulent velocity (blue). Parameters $\sigma_\infty = 1$, $\gamma = 1$, $\xi = 0.025$, $r_{\rm cir} = 10^3 r_{\rm g}$. Relativistic 1-T equation of state is on Fig7a, non-relativistic 1-T EOS is on Fig7b.

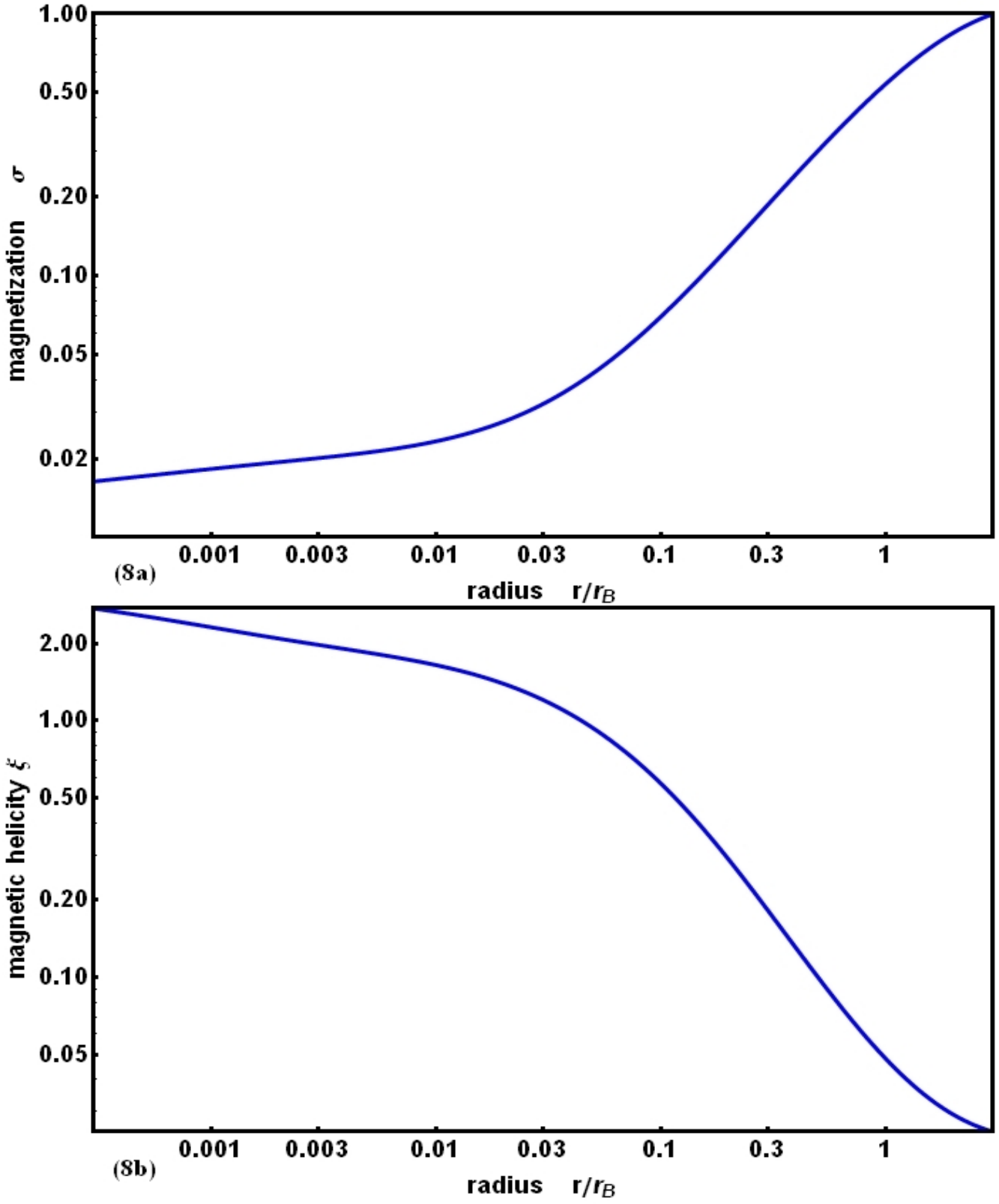

Fig. 8.— Magnetization σ verses dimensionless distance from the compact object r/r_B is on Fig8a. Dimensionless magnetic helicity ξ verses dimensionless distance from the compact object r/r_B is on Fig8b. Both are for **solution with angular momentum transport**. Circularization radius is $r_{\rm cir} = 10^3 r_{\rm g}$.